이학박사 학위논문

Magnetic Nanoparticle Manipulation through Ferromagnetic Micro-structure and Its Applications to Biosensors

강자성 마이크로 구조체를 통한 자성 나노입자의 움직임 제어와 바이오 센서에의 적용에 대한 연구

2019년 8월

서울대학교 대학원

물리천문학부

유 하 늘

Abstract

Magnetic Nanoparticle Manipulation through Ferromagnetic Micro-structure and Its Applications to Biosensors

Haneul Yoo

Department of Physics and Astronomy

The Graduate School

Seoul National University

Receptors in a biosensor have a role to fix the target substances to a sensor surface and are usually immobillized chemically on a sensor surface. In this biosensor, there are fundamental limitations that the detection speed of sensor depends on the diffusion speed of the target material in liquid, which leads to difficulties in the rapid disease diagnosis, high throughput screening. In addition, used receptor cannot be used again, and the entire sensor chip cannot be used again. In the case of a high-performance nano-biosensors have been studied recently, the manufacturing cost of the sensor chip is very high, thus a disposable sensor chip is a barrier to commercialization of the nano-biosensor. In this dissertation, we discuss

about methods to overcome the fundamental limitations of conventional bio-sensing systems.

First, a magnetically-focusing biochip structure enabling a single layered magnetic trap-and-release cycle for biosensors with an improved detection speed and selectivity was studied. Here, magnetic beads functionalized with specific receptor molecules were utilized to trap target molecules in a solution and transport actively *to* and *away from* the sensor surfaces to *enhance the detection speed* and *reduce the non-specific bindings*, respectively. Using our method, we demonstrated the high speed detection of IL-13 antigens with the improved detection speed by more than an order of magnitude. Furthermore, the release step in our method was found to reduce the non-specific bindings and improve the selectivity and sensitivity of biosensors.

Next, we studied a magnetically-refreshable receptor platform structure which can be integrated with quite versatile nano-biosensor structures to build *reusable* nano-biosensor chips. This structure allows one to easily remove used receptor molecules from a biosensor surface and reuse the biosensor for repeated sensing operations. Using this structure, we demonstrated reusable immunofluorescence biosensors. Significantly, since our method allows one to place receptor molecules very close to a nano-biosensor surface, it can be utilized to build reusable carbon nanotube transistor-based biosensors which require receptor molecules within a Debye length from the sensor surface. Furthermore, we also show that a

single sensor chip can be utilized to detect two different target molecules simply by replacing receptor molecules using our method.

Finally, we report a reusable and multi-detectable SPR sensor chip by fabricating a ferromagnetic nickel pattern on a conventional SPR sensor chip structure. The hysteresis property of ferromagnetic nickel pattern on our sensor chip enabled trapped magnetic nanoparticles on the SPR sensor chip by an external magnetic field and fixed them during a sensing process. Because receptor molecules were immobilized to the magnetic particles, our sensor chip could be reused through the removal of used magnetic particles and the trap of fresh magnetic particle. Thus, our single sensor chip could detect target molecules for 7 times without degradation of signals. Additionally, through the replacement of magnetic particles and receptors, our single sensor chip could detect two different target molecules.

Keywords: Magnetic Nanoparticle, CNT-FET, SPR Biosensor,
Ferromagnetism, Reusable Biosensor

Student Number: 2013-22990

Table of Contents

List of Figures

Chapter 1. Introduction

1.1. Biosensor

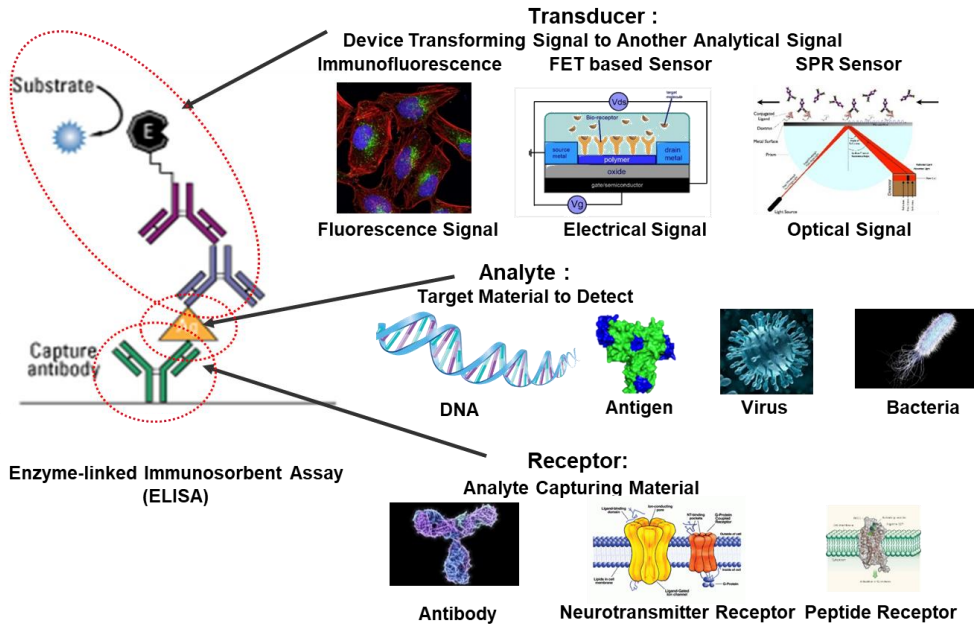

Figure 1-1. Major components of a biosensor.

Biosensors are devices to detect biochemical substance such as viruses, antigens, and DNAs.[1-22] They are extensively utilized for various practical fields such as healthcare, disease detection, industrial monitoring, and clinical analysis.[2, 3, 7, 8, 11, 13, 20, 23-30] Figure 1-1 shows the major components of a biosensor. Typically, biosensors are composed of receptors and transducers. Receptors selectively fix target biomaterials to sensor surfaces. Usually, materials used for receptors are selected according to the type of the target substances. For example, a corresponding antibody is used for the detection of antigen, and a corresponding DNA is used for detecting the DNA. Transducers convert binding signal from captured target material by the receptor into a recognizable signal. For example, a fluorescence-based biosensor performs detection through a fluorescent

signal when a fluorescent dye is labeled with a target substance. In the FET-based biosensors, the binding of target materials changes the electrical potential of the FET channel surface, which change the conductance of FET channel.[3, 21, 25, 27, 29, 31-34]

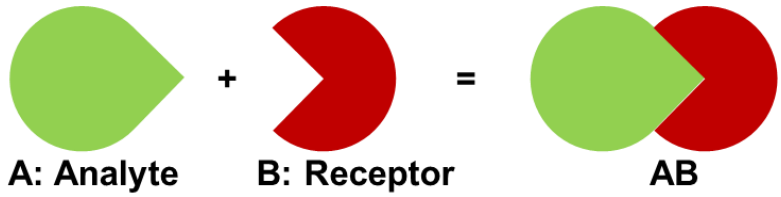

Figure 1-2. Binding reaction between an analyte and a receptor in a biosensor.

Figure 1-2 shows a scheme for binding reaction between an analyte and a receptor. The reaction can be explained by the following simple formula.[35]

$$A + B \rightleftharpoons AB \tag{1-1}$$

At this time, the reaction rate is proportional to the concentration of each component. After a sufficient period of time, the reaction reaches an equilibrium state as follows.

$$\frac{[A][B]}{[AB]} = \frac{k_d}{k_a} = K_D \tag{1-2}$$

,where K_d, K_a, K_D are called as dissociation rate, association rate, dissociation constant, respectively.

The quantity of total reaction by concentration of the target substance is

expressed by the following equation.

$$[AB] = \frac{[B_0][A]}{K_D + [A]} = \frac{[B_0]}{K_D/[A] + 1} \quad (1\text{-}3)$$

At this time, when the target concentration is injected by K_D, the reaction of the sensor reacts to about half of the maximum response of the sensor.(Figure 1-3)

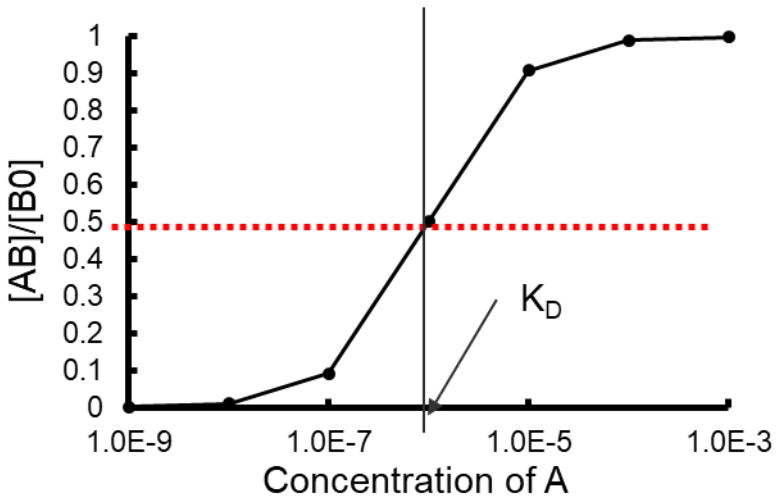

Figure 1-3. Dose dependence of target material.

1.2. Superparamagnetic Nano Particles and Its Manipulation

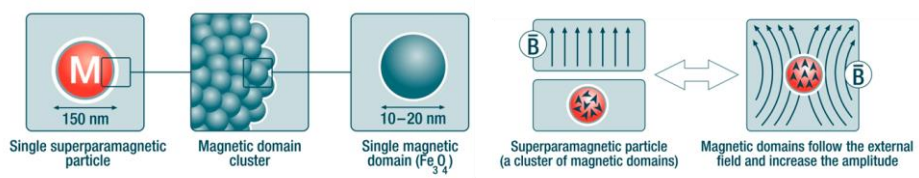

Figure 1-4. Structure and motion of superparamagnetic nanoparticles..

Superparamagnetic nano particles are usually composed of magnetic domains with sizes of about 10~20 nanometers.(Figure 1-4) Their magnetizations are aligned anisotropically when a magnetic field is not

applied. When a magnetic field is given, it is aligned in the direction of the magnetic field. Then magnetic forces on the magnetic particles are as follows

$$\vec{F}_m = V_p \vec{M} \nabla \vec{B} = \vec{m} \cdot \nabla \vec{B} \quad (1\text{-}4)$$

,where F, Vp, M, B, m mean force on magnetic nanoparticle, volume of nanoparticle, magnetization, magnetic moment, magnetic field, respectively. It can be seen from the equation that when the magnetic field is given, the magnetic particles move in the gradient direction of the intensity of a magnetic field. Through these properties, magnetic nanoparticles have been applied in many bio experiments. For example, it is usually used to separate certain materials from a mixed sample.

Figure 1-5. Magnetic separator.

Recently, there have been many studies to apply magnetic particles to biosensors. For example, it can be used for sensors such as NMR and for sensor labeling.[6] Magnetic particles were also used to amplify signals, improve detection speed, and reuse sensors.[4, 5, 24, 36-40]

1.3. References

[1] Chung J W, Kim S D, Bernhardt R and Pyun J C 2005 Application of SPR biosensor for medical diagnostics of human hepatitis B virus (hHBV) *Sensors and Actuators B: Chemical* **111-112** 416-22

[2] Clark M F and Adams A N 1977 Characteristics of the microplate method of enzyme-linked immunosorbent assay for the detection of plant viruses *J Gen Virol* **34** 475-83

[3] Gilbert P B, Gabriel E E, Miao X, Li X, Su S-C, Parrino J and Chan I S F 2014 Fold Rise in Antibody Titers by Measured by Glycoprotein-Based Enzyme-Linked Immunosorbent Assay Is an Excellent Correlate of Protection for a Herpes Zoster Vaccine, Demonstrated via the Vaccine Efficacy Curve *J. Infect. Dis.* **210** 1573-81

[4] Polyak B, Fishbein I, Chorny M, Alferiev I, Williams D, Yellen B, Friedman G and Levy R J 2008 High field gradient targeting of magnetic nanoparticle-loaded endothelial cells to the surfaces of steel stents *Proc Natl Acad Sci U S A* **105** 698-703

[5] Kim E, Oh J S, Ahn I S, Park K I and Jang J H 2011 Magnetically enhanced adeno-associated viral vector delivery for human neural stem cell infection *Biomaterials* **32** 8654-62

[6] Koh I, Hong R, Weissleder R and Josephson L 2008 Sensitive NMR sensors detect antibodies to influenza *Angew Chem Int Ed Engl* **47** 4119-21

[7] Teles F R R and Fonseca L R 2008 Trends in DNA biosensors *Talanta* **77** 606-23

[8] Tsang M K, Ye W, Wang G, Li J, Yang M and Hao J 2016 Ultrasensitive Detection of Ebola Virus Oligonucleotide Based on Upconversion Nanoprobe/Nanoporous Membrane System *ACS Nano* **10** 598-605

[9] Toh S Y, Citartan M, Gopinath S C B and Tang T-H 2015 Aptamers as a replacement for antibodies in enzyme-linked immunosorbent assay *Biosens. Bioelectron.* **64** 392-403

[10] He Y, Xie S, Yang X, Yuan R and Chai Y 2015 Electrochemical Peptide Biosensor Based on in Situ Silver Deposition for Detection of Prostate Specific Antigen *ACS Appl Mater Interfaces* **7** 13360-6

[11] Huygen K, Caboré R N, Maertens K, Van Damme P and Leuridan E 2015 Humoral and cell mediated immune responses to a pertussis containing vaccine in pregnant and nonpregnant women *Vaccine* **33** 4117-23

[12] Karlsson R, Michaelsson A and Mattsson L 1991 Kinetic analysis of monoclonal antibody-antigen interactions with a new biosensor based analytical system *J Immunol Methods* **145** 229-40

[13] Zhao Q, Duan R, Yuan J, Quan Y, Yang H and Xi M 2014 A reusable localized surface plasmon resonance biosensor for quantitative detection of serum squamous cell carcinoma antigen in

cervical cancer patients based on silver nanoparticles array *International journal of nanomedicine* **9** 1097-104
[14] Sulchek T, Friddle R W and Noy A 2006 Strength of multiple parallel biological bonds *Biophys J* **90** 4686-91
[15] Schwesinger F, Ros R, Strunz T, Anselmetti D, Güntherodt H-J, Honegger A, Jermutus L, Tiefenauer L and Plückthun A 2000 Unbinding forces of single antibody-antigen complexes correlate with their thermal dissociation rates *Proceedings of the National Academy of Sciences* **97** 9972-7
[16] Bhatia S K, Shriverlake L C, Prior K J, Georger J H, Calvert J M, Bredehorst R and Ligler F S 1989 Use of Thiol-Terminal Silanes and Heterobifunctional Crosslinkers for Immobilization of Antibodies on Silica Surfaces *Anal. Biochem.* **178** 408-13
[17] Heller M J, Forster A H and Tu E 2000 Active microelectronic chip devices which utilize controlled electrophoretic fields for multiplex DNA hybridization and other genomic applications *Electrophoresis* **21** 157-64
[18] Sheehan P E and Whitman L J 2005 Detection limits for nanoscale biosensors *Nano Lett* **5** 803-7
[19] Sassolas A, Leca-Bouvier B D and Blum L J 2008 DNA biosensors and microarrays *Chem Rev* **108** 109-39
[20] Karimi-Maleh H, Tahernejad-Javazmi F, Atar N, Lutfi M, Gupta V K and Ensafi A A 2015 A Novel DNA Biosensor Based on a Pencil Graphite Electrode Modified with Polypyrrole/Functionalized Multiwalled Carbon Nanotubes for Determination of 6-Mercaptopurine Anticancer Drug *Ind. Eng. Chem. Res.* **54** 3634-9
[21] Taylor J R, Fang M M and Nie S 2000 Probing specific sequences on single DNA molecules with bioconjugated fluorescent nanoparticles *Anal Chem* **72** 1979-86
[22] Jing P, Yi H Y, Xue S Y, Yuan R and Xu W J 2015 A 'signal on-off' electrochemical peptide biosensor for matrix metalloproteinase 2 based on target induced cleavage of a peptide *RSC Adv.* **5** 65725-30
[23] Lequin R M 2005 Enzyme immunoassay (EIA)/enzyme-linked immunosorbent assay (ELISA) *Clin Chem* **51** 2415-8
[24] Wignarajah S, Suaifan G A, Bizzarro S, Bikker F J, Kaman W E and Zourob M 2015 Colorimetric Assay for the Detection of Typical Biomarkers for Periodontitis Using a Magnetic Nanoparticle Biosensor *Anal Chem* **87** 12161-8
[25] Son M, Kim D, Park K S, Hong S and Park T H 2016 Detection of aquaporin-4 antibody using aquaporin-4 extracellular loop-based carbon nanotube biosensor for the diagnosis of neuromyelitis optica *Biosens Bioelectron* **78** 87-91
[26] Lacy E R 2012 Equilibrium and kinetic analysis of human interleukin-13 and IL-13 receptor alpha-2 complex formation *J Mol Recognit* **25** 184-91

[27] Ivnitski D, Abdel-Hamid I, Atanasov P and Wilkins E 1999 Biosensors for detection of pathogenic bacteria *Biosens. Bioelectron.* **14** 599-624
[28] Chen Q, Sun T, Song X, Ran Q, Yu C, Yang J, Feng H, Yu L and Wei D 2017 Flexible electrochemical biosensors based on graphene nanowalls for the real-time measurement of lactate *Nanotechnology* **28** 315501
[29] Liu Q, Wang J and Boyd B J 2015 Peptide-based biosensors *Talanta* **136** 114-27
[30] Choi S and Chae J 2009 Reusable biosensors via in situ electrochemical surface regeneration in microfluidic applications *Biosens. Bioelectron.* **25** 527-31
[31] Yao F, Duong D L, Lim S C, Yang S B, Hwang H R, Yu W J, Lee I H, Gunes F and Lee Y H 2011 Humidity-assisted selective reactivity between NO2 and SO2 gas on carbon nanotubes *Journal of Materials Chemistry* **21** 4502-8
[32] Li H, Mu X, Yang Y and Mason A J 2014 Low Power Multimode Electrochemical Gas Sensor Array System for Wearable Health and Safety Monitoring *IEEE Sensors Journal* **14** 3391-9
[33] Mishra R K, Hubble L J, Martin A, Kumar R, Barfidokht A, Kim J, Musameh M M, Kyratzis I L and Wang J 2017 Wearable Flexible and Stretchable Glove Biosensor for On-Site Detection of Organophosphorus Chemical Threats *ACS Sens* **2** 553-61
[34] Hicks K A 2015 Measuring Norfloxacin Binding to Trypsin Using a Fluorescence Quenching Assay in an Upper-Division, Integrated Laboratory Course *Journal of Chemical Education* **93** 380-2
[35] Karlsson R 1994 Real-time competitive kinetic analysis of interactions between low-molecular-weight ligands in solution and surface-immobilized receptors *Anal Biochem* **221** 142-51
[36] Robinson D A, Yoo J J, Castañeda A D, Gu B, Dasari R, Crooks R M and Stevenson K J 2015 Increasing the Collision Rate of Particle Impact Electroanalysis with Magnetically Guided Pt-Decorated Iron Oxide Nanoparticles *ACS Nano* **9** 7583-95
[37] Haun J B, Yoon T-J, Lee H and Weissleder R 2010 Magnetic nanoparticle biosensors *Wiley Interdiscip. Rev.: Nanomed. Nanobiotechnol.* **2** 291-304
[38] Koh I and Josephson L 2009 Magnetic Nanoparticle Sensors *Sensors* **9** 8130
[39] Orlov A V, Nikitin M P, Bragina V A, Znoyko S L, Zaikina M N, Ksenevich T I, Gorshkov B G and Nikitin P I 2015 A new real-time method for investigation of affinity properties and binding kinetics of magnetic nanoparticles *Journal of Magnetism and Magnetic Materials* **380** 231-5
[40] Rocha-Santos T A P 2014 Sensors and biosensors based on magnetic nanoparticles *TrAC Trends in Analytical Chemistry* **62** 28-36

Chapter 2. High-speed Active Biosensing using Nickel Patterned Structure and Magnetic Particle

2.1. Introduction

In biosensors, the binding of target molecules onto the specific receptor molecules fixed on sensor surfaces is detected by the transducer of the sensors.[1-6] Such a simple biosensor strategy has been extensively utilized for versatile bio- and medical applications. In most of conventional biosensors, a detection speed usually depends on the diffusion of target molecules in a solution. Thus, at a low concentration solution of target molecules, it may take a very long time for an enough number of target molecules to diffuse toward the sensor surfaces and to give a sensing signal.[7] For example, a reaction time between antibody and antigen proteins is about 2 hours in commercial enzyme-linked immunosorbent assay (ELISA).[8-10] However, for many practical applications such as point-of-care and emergency situations, it is highly important to reduce the detection time of biosensors.[11] There have been some previous efforts to actively drive target molecules to sensor surfaces using electric or magnetic methods instead of waiting for target molecular diffusion. For instance, target molecules such as nucleic acid and proteins can be guided toward a sensor element through the utilization of electrostatic fields from electrodes.[12] Additionally, magnetic field-assisted aggregation method was utilized for the trapping of target antigens.[13-16] Also, optomagnetic immunoassay technologies using magnetic beads and external magnetic fields were developed for the rapid detection of target molecules.[17-20] In

these methods, magnetic beads captured target in a solution and they were trapped and released repeatedly on a sensor surface by external magnetic fields, which increased the collision frequency between the target molecules and receptors on the sensor and enhanced the sensing speed. However, these methods often suffered from some limitations. For instance, electric fields to transport the biomolecules in solution may damage the target molecules. Magnetic field-assisted aggregation method was mainly utilized to concentrate the target solution, while it may increase the non-specific bindings and reduce the selectivity of the sensors. The repeated trap-and-release cycles via external magnetic fields may result in the aggregation of magnetic particles and limit the number of possible cycles.

Herein, we report a magnetically-focusing biochip structure for high-speed active biosensing with an improved selectivity. In this method, target molecules trapped by functionalized magnetic beads were driven repeatedly to (trapping) and away from (releasing) a functionalized ferromagnetic patterns on a biochip surface via magnetic field cycles, which increased the collision frequency between target molecules and sensor surfaces and enhanced its detection speed. Importantly, since magnetic field gradients occurred only near nickel patterns, the trapped magnetic beads formed a single layer on the sensor surface without forming a large aggregation, which minimized the degradation of the magnetic bead solution. Furthermore, the bindings of magnetic beads were highly focused only on the ferromagnetic patterns on the sensor surface, which allows us to

concentrate target molecules only on the sensor surfaces while avoiding non-specific binding on other surface area. Using this method, we demonstrated ~100 times faster detection speed compared with a conventional sandwich assay. Furthermore, the release step removed molecules bound to sensor surfaces non-specifically with weak binding forces, reducing the non-specific bindings by more than 50%. This strategy allows us to overcome the fundamental speed limitation of conventional passive sensors relying on target molecular diffusion. Furthermore, it minimizes the formation of magnetic bead aggregations and non-specific adsorption which often have been problems in magnetically-driven sensors. Since the sensing speed and selectivity of biochips are often critical in achieving high performance biosensors, our structures can be utilized for versatile bio- and medical applications.

2.1. Experimental Methods

2.1.1 Fabrication of nickel patterns on silicon substrate

Ferromagnetic nickel patterns (5 μm × 10 μm) were fabricated on a SiO_2 substrate (100 nm-thick SiO_2 film on a Si wafer) through conventional microfabrication processes. At first, a photoresist (AZ5214) layer was coated on the SiO_2 substrate using a spin coater (DONG AH TRADE CORP, ACE-200) and patterned via photolithography. Afterwards, a nickel film was thermally evaporated on the substrate, and the photoresist layer was rinsed with acetone. Under ambient conditions, we can expect the surface of

nickel was oxidized.[21] To reduce non-specific bindings on the nickel patterns, the additional layer of silicon oxide (50 nm) was chemically deposited to the surface of the substrate.

2.1.2 Experimental procedure for the magnetic trap-and-release cycles of superparamagnetic nanobeads on nickel patterned substrate

nanobeads (Nano-screenMAG-Streptavidin, hydrodynamic diameter of 100 nm) were purchased from Chemicell GmbH, Germany.[22] A nickel-patterned substrate was immersed in the 1% solution of BSA in a phosphate buffered saline (PBS) solution for 2 hr for the passivation of the substrate. For repeated magnetic trap-and-release cycle experiments, a flow cell was constructed by covering the substrate with a sheet of a cover glass using 3M double-sided tapes as a spacer. Then, it was placed on an inverted fluorescence microscope (TE2000U, Nikon, Japan) at a rhodamin channel. A solenoid (NS Magnet, Korea) which comprised 7500 turned electric wires and a 1.5 cm × 6.3 cm cylindrical iron core was purchased and placed on the stage of the microscope for generating external magnetic fields. Here, we generated magnetic fields following these four steps: *an upward magnetic field (150 mT), a downward magnetic field (35 mT), a downward magnetic field (150 mT)*, and *an upward magnetic field (35 mT)* for the *1st trap*, *1st release*, *2nd trap*, and *2nd release* of magnetic nanobeads. The strengths of applied magnetic fields were determined to achieve an efficient trapping and a clean release during the repeated cycles [23]. The movement and

distribution of magnetic beads were recorded by the fluorescence microscope.

2.1.3 Sensing operation of IL-13 antigen using magnetic trap-and-release cycle

Ready-set-go IL-13 ELISA Kit was purchased from eBioscience (USA). This kit is composed of IL-13 capture antibody (used as 2^{nd} antibody), biotinylated IL-13 detection antibody (used as 1^{st} antibody), and IL-13 antigen (used as target molecule). For the functionalization of a substrate with 2^{nd} antibodies, a nickel patterned substrate was subjected to a commonly used silanization technique.[24] First, the substrate was incubated in the 2% solution of 3-mercaptpropyltrimethoxysilane (MTS) in anhydrous toluene for 2 hr. Then, the substrate was thoroughly washed with anhydrous toluene and allowed to dry at a room temperature. To functionalize the silanized substrate with heterobifunctional linker molecules, organic hetrobifunctional crosslinker molecules (N-γ-maleimido-butyryloxy succinimide ester (GMBS)) were dissolved in 100 μl of dimethylformamide (DMF) and then diluted with ethanol to the final concentration of 2 mM. The silanized substrate was immersed in a cross-linker solution for 1 hr and washed three times with a PBS buffer. Afterward, 0.15 mg mL^{-1} solution of 2^{nd} IL-13 antibody in a PBS buffer was placed on the substrate and allowed to react for 2 hr at a room temperature. Residual unreacted antibodies were washed with a PBS buffer. Finally, the

substrate was immersed in the 1% solution of BSA in PBS for 2 hr to passivate antibody–free regions.[25] Afterwards, the substrate was placed on a microscope. The solution of biotin-labelled IL-13 antibodies from the ELISA kit was utilized for the conjugation of 1st antibodies and magnetic nanobeads. 100 μL solution of the magnetic nanobeads (0.1 mg mL^{-1} in PBS solution) was mixed with the 20 μL solution of the 1st antibody (1 mg mL^{-1} in PBS solution), and the mixed solution was incubated at a room temperature for 1 hr. 50 μL solution of IL-13 1st antibody functionalized magnetic nanobeads and IL-13 antigen mixture was injected to the flow cell. The concentrations of used IL-13 solution were 0.1 ng mL^{-1}, 1 ng mL^{-1} 10 ng mL^{-1} 100 ng mL^{-1}, and 200 ng mL^{-1}. The concentration of magnetic nanobeads for optimal results was determined by the control experiments (Figure 2-S1 in supplementary data). Note that the high concentration of magnetic nanobeads increased sensor signals, while it also increased non-specific binding due to the aggregation of the nanobeads. Afterwards, external magnetic fields were applied to perform the trap-and-release cycle for the detection of the antigen molecules. The movement and distribution of magnetic beads were recorded by the fluorescence microscope.

2.1.4 Conventional ELISA test procedure on the nickel patterned substrate

We prepared 2nd antibody-functionalized substrate through the same process as mentioned in the previous section. Then, the substrate was divided into small pieces (3 mm × 3 mm) to place into commonly used 96

well microplate. The wells with divided substrates were passivated by 1% solution of BSA for 2 hr and washed by wash buffer (TWEEN-20, 0.5% in PBS) for three times. After that, we placed 100 μl solutions of antigen on the nickel patterned substrate with different concentrations and incubated for given time intervals (0 min, 5 min, 10min, 20min, 30 min, 65 min and 95 min). After the incubation, the substrate was rinsed with the wash buffer for 3 times. Then, each substrate was incubated with 100 μl solution of secondary antibody for 1 hr and washed with the wash buffer for three times. Subsequently, the substrate was incubated in streptavidin labelled horse radish peroxidase (HRP) solution for 30 min and washed with the wash buffer for seven times. Afterward, the substrate was incubated in 3,3',5,5'-tetramethylbenzidine (TMB) solution of 100 μl and let to react for 15 min. Finally, the stop solution composed of 1 M phosphoric acid (50 μl) was added to stop the reaction, and the absorbance of the assay solution was obtained using a microplate reader.

2.3. High-speed Active Biosensing using Nickel Patterned Structure and Magnetic Particle

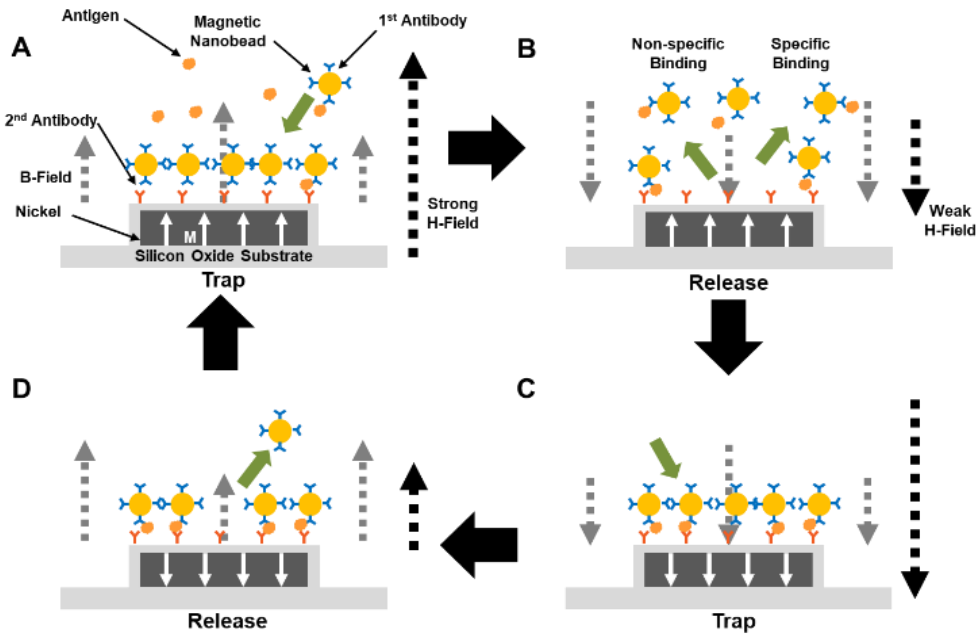

Figure 2-1. Schematic diagram depicting the magnetically-focusing biochip structures and the trap-and-release cycles using the structures for high speed biosensing. (A) 1st trapping step of magnetic nanobeads. An applied magnetic field in perpendicular direction to the substrate magnetized the nickel patterns, and thus total magnetic field above the nickel pattern became stronger than on other regions. Then the magnetic nanobeads were trapped on the nickel patterns and formed a single-layered structure. (B) 1st release step of magnetic nanobeads. A rather weak magnetic field in an opposite direction to previous magnetic fields was applied so that it did not change the magnetization direction of the patterns. Total magnetic fields above the nickel patterns became weaker than on other regions. Magnetic

nanobeads which did not form specific binding were released from the nickel patterns, while magnetic nanobeads which formed specific binding remained on the patterns. (C) 2nd trapping step of magnetic nanobeads. A rather strong magnetic field was applied and changed the magnetization direction of the patterns, and thus total magnetic field above the nickel patterns became stronger than on other regions. The magnetic nanobeads were trapped on the nickel patterns as a single layer. (D) 2nd release step of magnetic nanobeads. A rather weak magnetic field in opposite direction to the previous magnetic field was applied and did not change the magnetization direction of the patterns. Total magnetic fields above the nickel patterns became weaker than on other region. Magnetic nanobeads which did not form specific binding released on the nickel patterns, while magnetic nanobeads which formed specific binding remained on the patterns.

Figure 2-1 shows a schematic diagram depicting our active trapping strategy based on magnetically-focusing biochip structures. Detailed processes are presented in the experimental section. Briefly, ferromagnetic nickel patterns were fabricated on a sensor surface by a photolithography and a thermal evaporation process. The nickel patterns and substrate were covered with a SiO_2 layer through a chemical vapor deposition process.[26] Afterwards, 2^{nd} antibodies were immobilized on the sensor surface by a commonly-used

silanization technique. For the detection of target molecules, the solutions of target molecules and superparamagnetic nanobeads coated with a 1st antibody were introduced on the sensor surface. Here, due to the rather high concentration of magnetic beads, the target molecules were expected to bind to the 1st antibody on the bead surface rather quickly.[7] Then, the magnetic nanobeads were trapped onto the ferromagnetic pattern surfaces by applying a rather strong magnetic field (H-field, 150 mT) in a perpendicular direction to the sensor surface (Figure 2-1A). In this step, the external magnetic field magnetized the nickel patterns with the same direction as the magnetic field, and total magnetic fields (B-field) just above the patterns became stronger than those of other regions. Thus, the magnetic nanobeads were transported to and trapped on the nickel patterns due to magnetic field gradients, and the antigens attached on the magnetic beads might formed specific bindings with 2nd antibodies on the nickel patterns.[27, 28] Significantly, since such strong magnetic field gradients existed only near the nickel patterns, we could control the thickness of the trapped magnetic particles down to a *single layer* by adjusting the thickness of the patterns. In the following release step to remove non-specific bindings, a rather weak magnetic field (35 mT) was applied in an opposite direction to the previous applied magnetic field (Figure 2-1B). Here, the weak external magnetic field could not change the magnetization direction of the nickel patterns due to the

ferromagnetism of nickel, and total magnetic fields just above the patterns became weaker than those of other regions. Thus, the magnetic beads which did not form specific bindings on the ferromagnetic bindings were driven away from the nickel patterns. These trap-and-release cycles were repeated until we achieve a significant sensor signal (Figure 2-1C and 2-1D). As a proof of concepts, we measured the fluorescence intensity of magnetic bead accumulated on the nickel patterns during the release cycle as a sensor signal and used the signal to compare the detection speed of our strategy with that of conventional sensors. Note that the *trapping* step actively transported target molecules onto the sensor surface to *enhance the detection speed*, while the *releasing* step removed weakly-bound molecules from the sensor surface to *reduce the non-specific bindings*. Thus, this strategy can allow us to improve both detection speed and sensor selectivity. Furthermore, using a proper thickness of nickel patterns, we could trap a single layer of magnetic particles only onto specific sensor regions, which should have reduced the aggregation of magnetic particles.

2.4. Magnetic Trap and Release of Magnetic Particles on Nickel Pattern

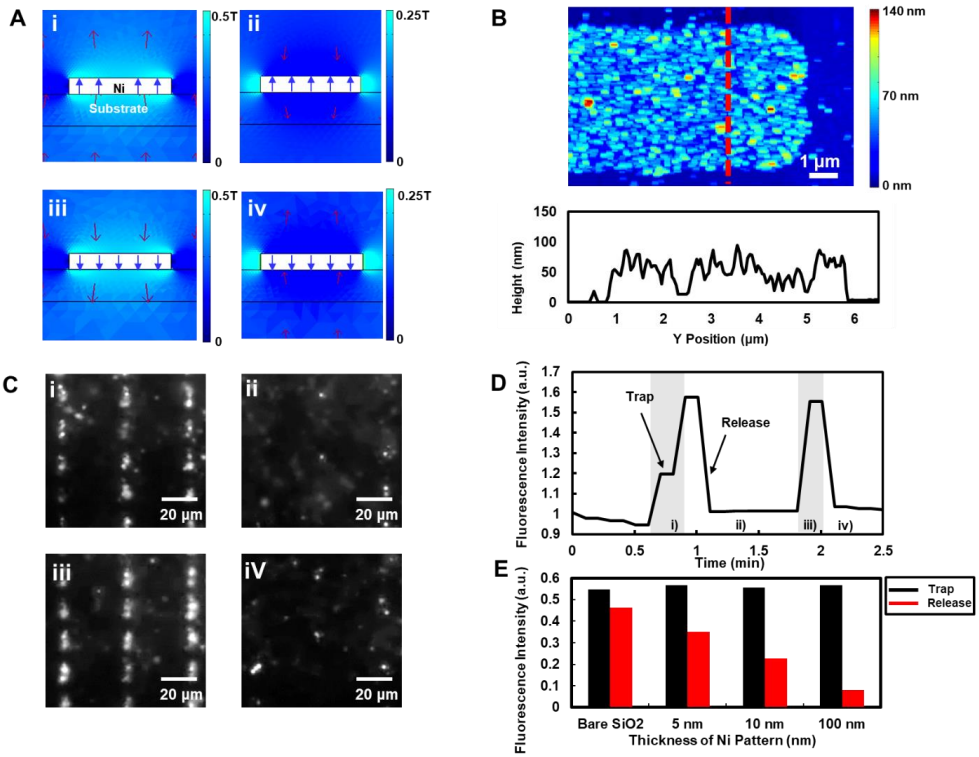

Figure 2-2. Trapping and releasing of a single layer of magnetic nanobeads on bare magnetically-focusing biochip structures. (A) Simulation results showing the total magnetic fields around a nickel pattern. Red arrows depict the direction and intensity of magnetic fields. Brighter blue regions represent the regions with a stronger magnetic fields. *i*), *ii*), *iii*), and *iv*) represent *1st trapping*, *1st release*, *2nd trapping*, *2nd release* cycles, respectively. (B) AFM image of single-layered magnetic nanobeads on a nickel pattern and cross section. A red-dotted line indicates the position of the cross section. (C) Fluorescence images of trap-and-release cycles on nickel patterns. *i*), *ii*), *iii*), and *iv*) represent *1st trapping*, *1st release*, *2nd*

trapping, *2nd release* cycles, respectively. The trapping times for *i*) and *iii*) were about *15 s* and *10 s*, respectively. The release times for *ii*) and *iv*) were about *45s* and *30s*, respectively. Brighter regions represent the distribution of fluorescence-dye-functionalized magnetic nanobeads. (D) Graph showing the fluorescence intensity change of microscope images during trap-and-release cycles of figure 2-2B. *Grey* and *white* regions indicate the *trapping* and *release* steps, respectively. (E) Bar graph showing the dependence of the trap-and-release efficiency on the nickel pattern thickness. *Black* and *red* bars indicate the fluorescence intensities of microscope images when the magnetic nanobeads were *trapped* and *released*, respectively.

Figure 2-2A depicts simulation results showing magnetic field intensities around a nickel structure when external magnetic fields were applied during trap-and-release cycles. The simulations were performed using COMSOL Multiphysics software at four different external magnetic field conditions which correspond to steps in Figure 2-1. When a strong external magnetic field was applied with an upward direction, the nickel structure was magnetized in the same direction to an external magnetic field (Figure 2-2A (i)). In this case, the magnetized nickel structure made magnetic fields just above the structure much stronger than in other regions (brighter region in Figure

2-2A (i)). Thus, we could expect that superparamagnetic nanobeads can be attracted toward the nickel structure because magnetic dipoles are driven to the regions with a stronger magnetic field (trapping step in Figure 2-1A).**[27, 28]** On the other hand, when a rather weak external magnetic field was applied with a downward direction which is opposite to the magnetization direction of the nickel structure, the magnetization direction of a nickel structure did not change because of the hysteresis of nickel (release step in Figure 2-2A (ii)). As a result, the magnetic field just above the structure became weaker than in other region. Thus, it is expected that the magnetic nanobeads can be released from the magnetized nickel structure, which corresponds to the 1st release in Figure 2-1. *Figure 2-2A (iii)* and *Figure 2-2A (iv)* show similar results which also correspond to the *2nd trap* and *2nd release* steps in Figure 2-1, respectively. These results show that the cycles of externals magnetic fields and hysteresis of nickel patterns can create proper magnetic field distribution for our trap-and-release cycle.

Figure 2-2B shows the AFM topography image and its cross section of a magnetically-focusing biochip structure after trapping process. A magnetic field of 150 mT was applied to a nickel patterned substrate and a magnetic nanobeads solution on the substrate. Afterwards, the surface of the dried substrate was measured by AFM. The image shows that most of nanobeads were trapped on the nickel

pattern due to the ferromagnetism of nickel. A cross section of red dotted line of the AFM image shows that the height of nanobeads was nearly uniform. These results indicate that the magnetic nanobeads formed a single layered structure on the nickel pattern without aggregations, which should have allowed the repeated trap-and-release without a minimal aggregation of magnetic beads.

Figure 2-2C shows the fluorescence microscopic images of fluorescence-labeled magnetic nanobeads (without antibody) trapped on nickel patterns of a magnetically-focusing biochip structure during trap-and-release cycles. Brightness represents the fluorescence intensity of fluorescence-labelled magnetic nanobeads on the substrate. It is showed that magnetic beads were concentrated to nickel patterns during 1^{st} and 2^{nd} trapping (Figure 2-2C (i) and (iii)). When a strong external magnetic field was applied in one direction that is perpendicular to the plane of the substrate, the magnetic nanobeads were drawn towards the nickel patterns on the substrate. On the other hand, it is shown that the magnetic nanobeads were dispersed in the solution during 1^{st} and 2^{nd} release steps (Figure 2-2C (ii) and (iv)). When a rather weak external magnetic field was applied in an opposite direction, most of the magnetic nanobeads were pushed away from the nickel patterns, which decreased the fluorescence intensity. For the quantified analysis, the fluorescence intensity of each frame was measured and plotted in Figure 2-2D. In the trapping step, the

fluorescence intensity increased quickly. In the release step, the fluorescence intensity was recovered quickly back to its original values. These result indicates we can repeat the trap-and-release cycle without causing degradations or damages of our sensors.

Figure 2-2E shows fluorescence intensity changes of the magnetic nanobeads on the nickel patterns during the trap-and-release cycles using a bare SiO_2 substrate or nickel patterns with different thickness of 5 nm, 10nm, and 100 nm. In bare substrate without ferromagnetic patterns, trapped magnetic nanobeads were not much released from the substrate during the release step. On the other hand, as nickel thicknesses increased, the amounts of released magnetic nanobeads increased, providing a clear contrast. These results shows that the nickel patterns play an important role in releasing magnetic nanobeads from the sensor surface, which can be critical in removing non-specifically-bound nanobeads from the sensor surface.

2.5. Detection Speed Enhancement by Trap and Release of Magnetic Particle

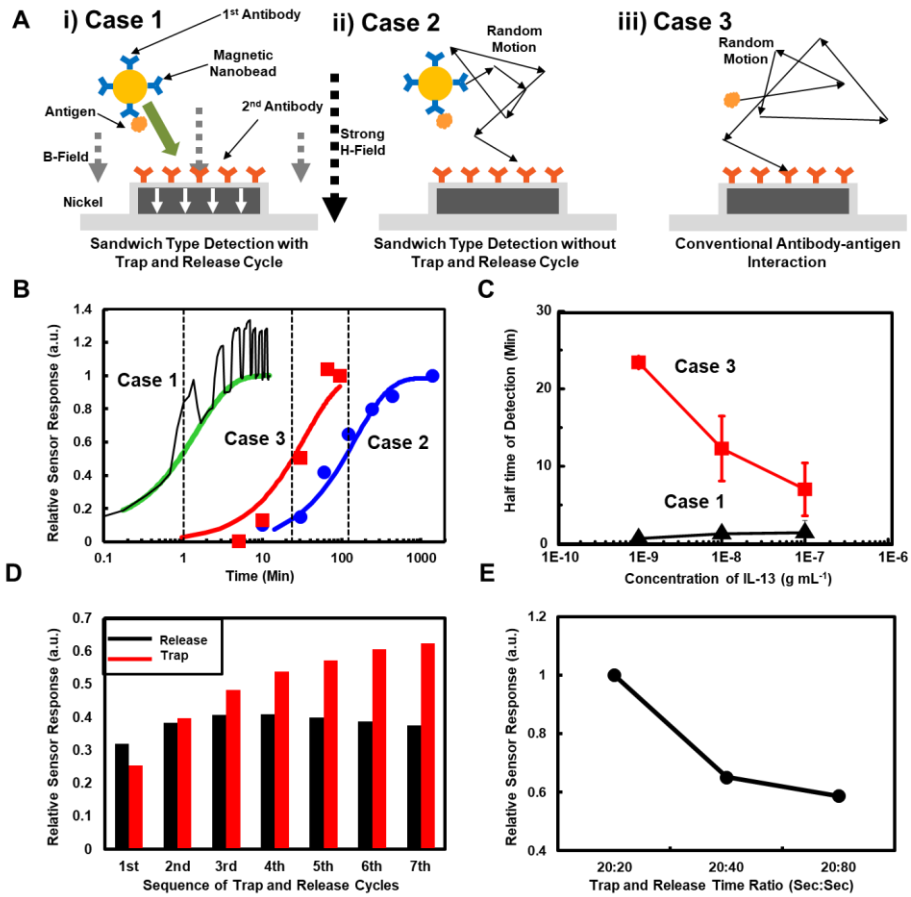

Figure 2-3. High-speed detection using functionalized magnetically-focusing biochip structures. (A) three different schemes of antigen detections: (i) sandwich type detection with trap-and-release cycle, (ii) sandwich type detection without trap-and-release cycle, and (iii) conventional antibody-antigen interactions. (B) Normalized reaction graph from the detection experiments using the methods of 3A (i), (ii), and (iii). (C) Half-time of detection using different concentration solutions of IL-13 antigens. Black and red dots indicate the data with or without the trap-and-

release cycles, respectively. (D) Accumulated differences of the fluorescence intensities during the trap (red bars) and release periods. The 100 ng mL-1 of IL-13 antigen solution was used as a target solution. (E) Relative sensor responses by the sandwich assay with trap-and-release cycles with different ratio of trap-and-release times.

Figure 2-3A shows schematic diagrams depicting three different antigen detection experiments performed to demonstrate the improved detection speed of our sensing strategy. Figure 2-3A (i) shows our detection process with trap-and-release cycles on a magnetically-focusing biochip structure explained in the Figure 2-1. Here, we utilized 1^{st} and 2^{nd} antibodies of IL-13 to functionalize *magnetic nanobeads* and *nickel patterns*, respectively. We repeated trap-and-release cycles while recording the fluorescence intensity of the fluorescence-labelled magnetic nanobeads on the nickel patterns by the CCD camera in the fluorescence microscope. Figure 2-3A (ii) shows a sandwich type detection method using the same materials without trap-and-release cycles. In this case, both target molecules and magnetic beads should diffuse randomly until they bind to the sensor surface just like conventional sandwich assays. We also measure the binding speed when only antigens bind with antibody without magnetic beads (Figure 2-3A (iii)). In this case, the antigens diffuse randomly to be trapped on the antibodies of the sensor surfaces, and

the amount of bound antigens was estimated using the conventional ELISA method.[29-31]

Figure 2-3B shows a normalized reaction graph during three different experiments of IL-13 antigen detection as shown in Figure 2-3A. The black line depicts normalized fluorescence intensities during the sandwich type detection with trap-and-release cycles (case 1). *Trapping* and *release* times were *50* s and *50* s, respectively. Note that the intensities were rapidly *increased* and *decreased* over the time, which were caused by the *trapping* and *release* of magnetic nanobeads by the nickel patterns, respectively. When rather strong magnetic fields were applied, magnetic nanobeads were attracted to a nickel pattern so that fluorescence intensity increased. On the other hands, fluorescence intensity decreased in the release step because of the release of magnetic nanobeads which were not bound to 2^{nd} antibodies on the sensor surface. As the trap and release steps were repeated, the overall fluorescence levels increased, indicating the selective binding of target molecules and magnetic beads on the sensor surfaces. Here, we utilized the fluorescence intensity values at *release* steps as a sensor signal because magnetic beads can remain on the sensor surface non-specifically by magnetic fields in trapping steps. *Blue* and *red* dots represent the experimental results of the *sandwich detection without trap-and-release cycles* (*case 2*) and target detection *via* ELISA (*case 3*), respectively. We utilized *1* ng/mL, *100* ng/mL, and *1*

ng/mL solutions of IL-13 antigen as a target solution for the case *1*, *2*, and *3*, respectively. The reaction graph can be fitted using the exponential decay model like, [32]

$$\mathbf{N(t)} = \boldsymbol{N_0}\left(\mathbf{1} - \boldsymbol{e}^{-\boldsymbol{t}/\boldsymbol{\tau}}\right) \quad (1)$$

$$\boldsymbol{t_{1/2}} = \boldsymbol{\tau}\mathbf{ln(2)} \quad (2)$$

where, N_0, $N(t)$, τ, and $t_{1/2}$ indicate the *quantity of saturated response*, *a sensor response*, *a time constant*, and *half-time which is relevant to a saturation time*, respectively. The *green*, *blue*, and *red* lines in Figure 2-3B are fitting curves for case *1*, case *2*, and case *3*, respectively. The half-time represents the time when the level of sensor response is a half of the saturated response. The estimated half-time for the sandwich assays *with (case 1)* or *without (case 2)* the trap-and-release cycles were *~1.2* min and *~107* min, respectively. Also, it should be mentioned that the concentration of the target solution for case 2 (without trap-and-release cycles) was 100 times higher than that of case 1 (with the cycles). It clearly shows that the trap-and-release cycles can enhance the detection speed by more an order of magnitude even in a very low concentration target solution. The case 3 represents the reaction graph only for target antigen bindings, and its half time was estimated as ~23.5 min. However, to achieve the detection signals,

it required additional processes such as the binding of 2nd antibody and enzyme, and enzymatic reactions, which takes about 100 min. Thus, the effective half-time including entire process can be ~120 min, which is much longer than that of the trap-and-release cycle-based detection in case 1. It indicates that the *entire detection time for our method* can be even shorter than *the time only for the binding of only target antigens with a much higher concentration*.

Figure 2-3C shows the half-time values for the reactions with various concentrations of IL-13 antigen in the sandwich detection experiments with (case 1, black triangles) or without (case 2, red square) trap-and release cycles. Note that the half-time values for the detection experiments without trap-and-release cycles (case 3) *decreased* as the target concentration *increased*. Previous works show that the detection time for conventional passive sensors can be very long in a rather low concentration target solution [30]. It is because in low concentration solution, only a small number of target molecules diffuse randomly, and it takes a rather long time for the sensor surface to capture enough number of diffusion target molecules for sensing signals. On the other hand, the detection time with our trap-and-release cycles does not change much at different concentration solutions. Presumably, it is because our method uses a number of magnetic beads to capture target molecules and bring them actively to the sensor surfaces, which does not rely on the random diffusion of target

molecules. And, thus, the detection speed of our detection method is not limited by the fundamental limitations of conventional passive sensors relying on molecular diffusion.

Figure 2-3D shows the accumulated differences of sensor signals after each trap (red bars) and release (black bars) step. Here, we first measured the differences before and after each trap or release step, and they were accumulated up to a specific step to calculate the accumulated difference value for the step. The 100 ng mL^{-1} of IL-13 antigen solution was used as a target solution. Since the magnetic forces tend to move magnetic beads away from the sensor surface in the release step, the accumulated difference data of the release step represent the target binding mainly by random diffusion of target molecules. On the other hand, since magnetic beads with captured target molecules were driven to the sensor surface by magnetic fields in the trapping steps, the data of the trapping step represents the detection by active trapping. Note that the diffusion driven binding has a rather large portion in the first cycle, presumably because the biochemical reaction speed is commonly fastest when the reaction is started. However, as the cycles were repeated, the target binding by random molecular diffusion was slowed down and saturated (black bars), while more target antigens were captured on the sensor surface by active trapping *via* magnetic forces (red bars). These results imply that the active transport process of antigens in our strategy can, in

effect, accelerate antibody-antigen reaction speed and allow us to overcome the fundamental speed limitations of conventional bio-sensors based on molecular diffusion.

We performed the detection experiments with different time periods of trapping or release steps (Figure 2-3E). Here, we measured the response of our sensor by changing the release times as 20 s, 40 s, and 80 s with a trap time of 20 s. Then, the sensor responses were measured after repeated trap-and-release cycles for 12 min. The concentration of IL-13 target antigen solution was 10 ng mL^{-1}. Note that the sensor response with a relatively shorter release time has larger sensor signals even with the same total reaction time. This result indicates that the active trapping during the trapping step gives a major contribution for the sensor responses in our method, which is also consistent with the result in Figure 2-3D.

2.6. Improved Selectivity of Magnetically-focusing Biochip Structures

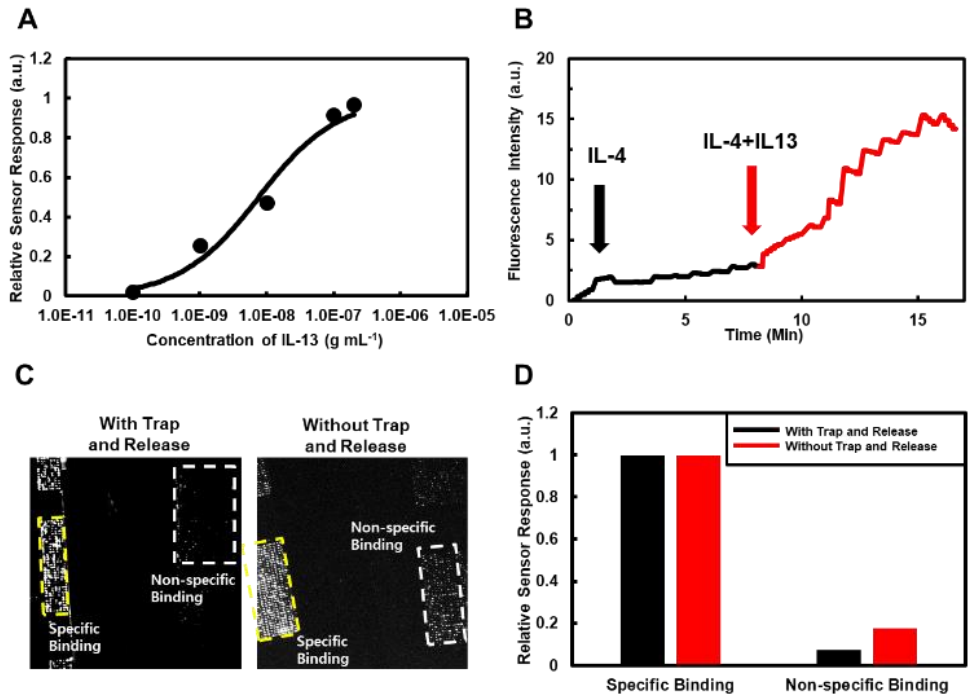

Figure 2-4. Improved selectivity via magnetically-focusing biochip structures. (A) Normalized sensor response curves with different concentrations of IL-13 antigens by sandwich assay with trap-and- release cycles. (B) Real time response curves in mixed samples. Black line depicts the injection of IL-4 which is for a negative control, and red line depicts the injection of IL-13 which is a specific target. (C) Fluorescence images after the sandwich assay of IL-13 with or without trap-and-release cycles on the substrates including the regions of different molecular layers. The regions marked by “Specific Binding” was coated with 1st antibody of IL-13. The regions marked by “Non-specific Binding” was coated with BSA. (D)

Normalized fluorescence intensities measured from the regions marked by yellow and white squares in Figure 2-4C. The measured intensity was normalized by that of the specific binding regions.

Figure 2-4A shows a graph depicting the normalized response curves of our detection experiments with different target concentrations ranging from 0.1 ng mL^{-1} to 200 ng mL^{-1}. Here, we performed the detection experiments using our trap-and-release cycles on magnetically-focusing biochip structures and normalized the sensor response data by saturated values. The result was fitted by the Langmuir isotherm model (black line) to estimate the binding constant K_d.[33, 34] The K_d value estimated from the fitting curve was 8.9 ± 2.08 ng mL^{-1}, which is consistent with the results reported previously.[35] Also, note that the standard deviation of the measured K_d value was about ~23%, which is similar to those measured by conventional fluorescence assay or SPR methods based on the static equilibrium of molecular bindings.[35, 36] Previous works also show versatile advanced measurement methods relying on dynamic processes. For example, AFM or optical tweezer methods using the dynamic motions of nanoprobes or beads have been utilized to measure K_d values with different distributions. In this case, such distributions of the measured data were attributed to various factors such as the multivalency of used probes and the probe velocity at the release step.[37, 38] Previously, it was reported that the multivalancy of antibody-antigen interactions on the probe surfaces affects the dissociation

rate and causes a rather large distribution of K_d.[39] The standard deviation of K_d values measured by some previous AFM methods using a rather high-density molecular layer on the probe was about 50~100%.[37, 40] However, in our case, the estimated number of attached antibodies on the beads was only 15 ~ 20 and, thus, the surface coverage of antibodies on our magnetic beads was just 2%. Considering that previous optical tweezer experiments with a similar small surface coverage resulted in a rather small distribution of the measured data close to our results, we can expect the multivalency effect in our experiment did not significantly increase the distribution of our data.[23, 41] Furthermore, in AFM or optical tweezer measurements, the unbinding force rate during the K_d measurement can significantly affect the measured data, often resulting in a rather large distribution in the measured data.[42] However, the force applied to the bead during the release step in our experiments was estimated as only ~1 pN which was much smaller that the common unbinding forces of about 50-100 pN between ab-ag and should not break the specific bindings between the beads and sensor surfaces.[37, 43]. Since our process does not unbind the molecules, the effect of bead speeds on the distribution of measured data should be small, and we can analyze our measurement data like conventional sandwich assay processes. In a common sandwich assay, the 1st and 2nd antibodies can have different K_d values. In this case, the dose-dependent reaction curves are mainly determined by the first reaction (Figure 2-S2, and Table 2-S1 in supplementary data). In our detection experiment, the target antigens should

first bind to the 1st antibody on the magnetic beads in solution, and they were driven to the sensor surface for the binding to the 2nd antibody. Thus, the responses curves in our method should be determined mainly by the 1st antibody reactions on the magnetic beads. Previous works and our control experiments using SPR methods showed a trend that the K_d value of the 1st antibody for IL-13 was approximately ~10 times larger than that of 2nd antibody at given reaction conditions.(Figure 2-S3 in supplementary data)[44] Interestingly, in case 3 where target antigens bound first to the 2nd antibody, the estimated K_d value of ~1 ng mL^{-1} was 10 times smaller than that of case 1 (Figure 2-S4 in supplementary data). This trend is also consistent with the results reported previously and those obtained in our SPR control.

Figure 2-4B shows normalized fluorescence intensity changes in the detection experiment using mixed antigen solution. Detailed processes are in the experimental section. Briefly, the solution of IL-4 antigen (10 ng mL^{-1}) was first injected to the IL-13 antibody- functionalized sensor surface for a negative control, and the detection processes were performed using the trap-and-release cycle with IL-13 antibody functionalized magnetic beads (black line). Then, the solution of IL-13 antigen (10 ng mL^{-1}) was introduced to the substrate for the positive control, and we performed sensing experiments using the trap-and-release cycle for 9 min (red line). Note that the IL-13 reaction was performed in the mixed solution of IL-13 and IL-4 antigens. The sensor signals did not change much when the non-

specific IL-4 was injected. However, the injection of specific IL-13 target antigen rapidly increased the sensor signals even in the mixed solution of IL-13 and IL-4. It shows that our sensor can selectively detect specific target molecules even in a mixed solution.

We prepared a substrate including the regions functionalized with two different molecular layers and performed the detection experiments with (left image in Figure 2-4C) or without (right image in Figure 2-4C) the trap-and-release cycles on the magnetically-focusing biochip structures. Detailed procedures are presented in the experimental section. In brief, one substrate was functionalized with IL-13 and passivated with bovine serum albumin (BSA), and another one was only passivated with BSA. The two substrates were attached close on the clean silicon substrate by double sided tape. IL-13 antigens (100 ng mL^{-1}) and magnetic bead with IL-13 antibody were utilized for the detection experiments. The *trap* and *release* times for the trap-and-release cycles were *10 s* and *50 s*, respectively. Note that in both cases, we observed a large fluorescence intensity on the regions functionalized with IL-13 antibodies (marked by “specific binding”), indicating specific bindings. However, we could observe a much smaller fluorescence intensity on the regions with BSA (marked by “non-specific binding”) when the detection experiment was performed *with* a trap-and-release cycle (left image in Figure 2-4C) than those without it (right image in Figure 2-4C). Figure 2-4D shows the normalized fluorescence intensities in the squares of 4C, which allows us to compare the portion of non-specific

binding (white squares) with respect to the specific bindings (yellow squares). Black bars represent the results of detection with trap-and-release, and red bars represent the results of detection without trap-and-release. Note that the relative intensity by non-specific binding decreased by ~60% when the trap-and-release cycles were performed. Presumably, since the non-specific binding forces were usually much weaker than specific binding forces, and magnetic beads were on the nickel patterns as a single layer, the magnetic fields in the release cycles removed only non-specifically bound magnetic beads from the sensor surfaces while leaving specifically bound beads. Note that, for developing a highly-sensitive biosensing method, it is critical to increase its signal-to-noise ratio by reducing noises such as non-specific bindings as well as signal noises.[45, 46] Our method exhibited reduced non-specific bindings while maintaining a similar K_d value for selective bindings. This result indicates that our sensing method can operate at a lower target concentration than conventional methods and thus has, in effect, an improved sensitivity for practical applications.

2.7. Summary

In conclusion, we developed a magnetically-focusing biochip structure to actively drive target molecules onto the specific regions of sensor surfaces for the high speed biosensing with an improved selectivity. As a proof of concept, we performed the sandwich assay of the IL-13 antigens with trap-and-release cycles and showed that the trap-and-release cycles in

our method can enhance its detection speed by more than orders of magnitude. Furthermore, we also demonstrated that the release of single layered magnetic beads in our method could reduce non-specific bindings and the aggregation of magnetic beads, improving the selectivity of biosensors. Considering that our method allowed us to overcome the fundamental limitations of conventional biosensors in terms of its speed and selectivity, it should open up versatile biomedical applications such as highly-sensitive and ultra-fast point-of-care systems.

2.8. References

[1] Liu Q, Wang J and Boyd B J 2015 Peptide-based biosensors *Talanta* **136** 114-27

[2] Jing P, Yi H Y, Xue S Y, Yuan R and Xu W J 2015 A 'signal on-off' electrochemical peptide biosensor for matrix metalloproteinase 2 based on target induced cleavage of a peptide *RSC Adv.* **5** 65725-30

[3] He Y, Xie S, Yang X, Yuan R and Chai Y 2015 Electrochemical Peptide Biosensor Based on in Situ Silver Deposition for Detection of Prostate Specific Antigen *ACS Appl Mater Interfaces* **7** 13360-6

[4] Teles F R R and Fonseca L R 2008 Trends in DNA biosensors *Talanta* **77** 606-23

[5] Karimi-Maleh H, Tahernejad-Javazmi F, Atar N, Lutfi M, Gupta V K and Ensafi A A 2015 A Novel DNA Biosensor Based on a Pencil Graphite Electrode Modified with Polypyrrole/Functionalized Multiwalled Carbon Nanotubes for Determination of 6-Mercaptopurine Anticancer Drug *Ind. Eng. Chem. Res.* **54** 3634-9

[6] Sassolas A, Leca-Bouvier B D and Blum L J 2008 DNA biosensors and microarrays *Chem Rev* **108** 109-39

[7] Nair P R and Alam M A 2010 Theoretical detection limits of magnetic biobarcode sensors and the phase space of nanobiosensing *Analyst* **135** 2798-801

[8] Reen D J 1994 *Basic Protein and Peptide Protocols,* ed J M Walker (Totowa, NJ: Humana Press) pp 461-6

[9] Lequin R M 2005 Enzyme immunoassay (EIA)/enzyme-linked immunosorbent assay (ELISA) *Clin Chem* **51** 2415-8

[10] Clark M F and Adams A N 1977 Characteristics of the microplate method of enzyme-linked immunosorbent assay for the detection of plant viruses *J Gen Virol* **34** 475-83

[11] Sheehan P E and Whitman L J 2005 Detection limits for nanoscale biosensors *Nano Lett* **5** 803-7
[12] Heller M J, Forster A H and Tu E 2000 Active microelectronic chip devices which utilize controlled electrophoretic fields for multiplex DNA hybridization and other genomic applications *Electrophoresis* **21** 157-64
[13] Koh I, Hong R, Weissleder R and Josephson L 2008 Sensitive NMR sensors detect antibodies to influenza *Angew Chem Int Ed Engl* **47** 4119-21
[14] Haun J B, Yoon T-J, Lee H and Weissleder R 2010 Magnetic nanoparticle biosensors *Wiley Interdiscip. Rev.: Nanomed. Nanobiotechnol.* **2** 291-304
[15] Koh I and Josephson L 2009 Magnetic Nanoparticle Sensors *Sensors* **9** 8130
[16] Rocha-Santos T A P 2014 Sensors and biosensors based on magnetic nanoparticles *TrAC Trends in Analytical Chemistry* **62** 28-36
[17] Bruls D M, Evers T H, Kahlman J A H, van Lankvelt P J W, Ovsyanko M, Pelssers E G M, Schleipen J J H B, de Theije F K, Verschuren C A, van der Wijk T, van Zon J B A, Dittmer W U, Immink A H J, Nieuwenhuis J H and Prins M W J 2009 Rapid integrated biosensor for multiplexed immunoassays based on actuated magnetic nanoparticles *Lab on a Chip* **9** 3504-10
[18] Dittmer W U, Evers T H, Hardeman W M, Huijnen W, Kamps R, de Kievit P, Neijzen J H M, Nieuwenhuis J H, Sijbers M J J, Dekkers D W C, Hefti M H and Martens M F W C 2010 Rapid, high sensitivity, point-of-care test for cardiac troponin based on optomagnetic biosensor *Clinica Chimica Acta* **411** 868-73
[19] Morozov V N, Groves S, Turell M J and Bailey C 2007 Three Minutes-Long Electrophoretically Assisted Zeptomolar Microfluidic Immunoassay with Magnetic-Beads Detection *J. Am. Chem. Soc.* **129** 12628-9
[20] Morozov V N and Morozova T Y 2006 Active bead-linked immunoassay on protein microarrays *Analytica Chimica Acta* **564** 40-52
[21] De Los Santos Valladares L, Ionescu A, Holmes S, Barnes C H W, Bustamante Domínguez A, Avalos Quispe O, González J C, Milana S, Barbone M, Ferrari A C, Ramos H and Majima Y 2014 Characterization of Ni thin films following thermal oxidation in air *Journal of Vacuum Science & Technology B, Nanotechnology and Microelectronics: Materials, Processing, Measurement, and Phenomena* **32**
[22] Kim E, Oh J S, Ahn I S, Park K I and Jang J H 2011 Magnetically enhanced adeno-associated viral vector delivery for human neural stem cell infection *Biomaterials* **32** 8654-62

[23] Yoo H, Lee D J, Cho D G, Park J, Nam K W, Cho Y T, Park J Y, Chen X and Hong S 2016 Magnetically-refreshable receptor platform structures for reusable nano-biosensor chips *Nanotechnology* **27** 045502
[24] Bhatia S K, Shriverlake L C, Prior K J, Georger J H, Calvert J M, Bredehorst R and Ligler F S 1989 Use of Thiol-Terminal Silanes and Heterobifunctional Crosslinkers for Immobilization of Antibodies on Silica Surfaces *Anal. Biochem.* **178** 408-13
[25] Taylor J R, Fang M M and Nie S 2000 Probing specific sequences on single DNA molecules with bioconjugated fluorescent nanoparticles *Anal Chem* **72** 1979-86
[26] Furuya M, Haramura M and Tanaka A 2006 Reduction of nonspecific binding proteins to self-assembled monolayer on gold surface *Bioorg Med Chem* **14** 537-43
[27] Urbach A R, Love J C, Prentiss M G and Whitesides G M 2003 Sub-100 nm confinement of magnetic nanoparticles using localized magnetic field gradients *J Am Chem Soc* **125** 12704-5
[28] Polyak B, Fishbein I, Chorny M, Alferiev I, Williams D, Yellen B, Friedman G and Levy R J 2008 High field gradient targeting of magnetic nanoparticle-loaded endothelial cells to the surfaces of steel stents *Proc Natl Acad Sci U S A* **105** 698-703
[29] Gan S D and Patel K R 2013 Enzyme Immunoassay and Enzyme-Linked Immunosorbent Assay *Journal of Investigative Dermatology* **133** 1-3
[30] Toh S Y, Citartan M, Gopinath S C B and Tang T-H 2015 Aptamers as a replacement for antibodies in enzyme-linked immunosorbent assay *Biosens. Bioelectron.* **64** 392-403
[31] Gilbert P B, Gabriel E E, Miao X, Li X, Su S-C, Parrino J and Chan I S F 2014 Fold Rise in Antibody Titers by Measured by Glycoprotein-Based Enzyme-Linked Immunosorbent Assay Is an Excellent Correlate of Protection for a Herpes Zoster Vaccine, Demonstrated via the Vaccine Efficacy Curve *J. Infect. Dis.* **210** 1573-81
[32] Cao W and De La Cruz E M 2013 Quantitative full time course analysis of nonlinear enzyme cycling kinetics *Sci Rep* **3** 2658
[33] Lee M, Jung J W, Kim D, Ahn Y J, Hong S and Kwon H W 2015 Discrimination of Umami Tastants Using Floating Electrode-Based Bioelectronic Tongue Mimicking Insect Taste Systems *ACS Nano* **9** 11728-36
[34] Son M, Kim D, Park K S, Hong S and Park T H 2016 Detection of aquaporin-4 antibody using aquaporin-4 extracellular loop-based carbon nanotube biosensor for the diagnosis of neuromyelitis optica *Biosens Bioelectron* **78** 87-91

[35] Lacy E R 2012 Equilibrium and kinetic analysis of human interleukin-13 and IL-13 receptor alpha-2 complex formation *J Mol Recognit* **25** 184-91
[36] Hicks K A 2015 Measuring Norfloxacin Binding to Trypsin Using a Fluorescence Quenching Assay in an Upper-Division, Integrated Laboratory Course *Journal of Chemical Education* **93** 380-2
[37] Schwesinger F, Ros R, Strunz T, Anselmetti D, Güntherodt H-J, Honegger A, Jermutus L, Tiefenauer L and Plückthun A 2000 Unbinding forces of single antibody-antigen complexes correlate with their thermal dissociation rates *Proceedings of the National Academy of Sciences* **97** 9972-7
[38] Gautier H O B, Thompson A J, Achouri S, Koser D E, Holtzmann K, Moeendarbary E and Franze K 2015 *Methods in Cell Biology*, ed E K Paluch: Academic Press) pp 211-35
[39] Howarth M, Chinnapen D J F, Gerrow K, Dorrestein P C, Grandy M R, Kelleher N L, El-Husseini A and Ting A Y 2006 A monovalent streptavidin with a single femtomolar biotin binding site *Nature methods* **3** 267-73
[40] Sulchek T, Friddle R W and Noy A 2006 Strength of multiple parallel biological bonds *Biophys J* **90** 4686-91
[41] Stout A L 2001 Detection and Characterization of Individual Intermolecular Bonds Using Optical Tweezers *Biophysical Journal* **80** 2976-86
[42] Neuman K C and Nagy A 2008 Single-molecule force spectroscopy: optical tweezers, magnetic tweezers and atomic force microscopy *Nat Methods* **5** 491-505
[43] El-Kirat-Chatel S, Mil-Homens D, Beaussart A, Fialho A M and Dufrene Y F 2013 Single-molecule atomic force microscopy unravels the binding mechanism of a Burkholderia cenocepacia trimeric autotransporter adhesin *Mol Microbiol* **89** 649-59
[44] Huygen K, Caboré R N, Maertens K, Van Damme P and Leuridan E 2015 Humoral and cell mediated immune responses to a pertussis containing vaccine in pregnant and nonpregnant women *Vaccine* **33** 4117-23
[45] Chung J W, Kim S D, Bernhardt R and Pyun J C 2005 Application of SPR biosensor for medical diagnostics of human hepatitis B virus (hHBV) *Sensors and Actuators B: Chemical* **111-112** 416-22
[46] Samuel P M, Abdellah M, Haibo L, Carmen A M, Robert M, Derek A, Jesper M and Zhang X C 2002 Label-free bioaffinity detection using terahertz technology *Physics in Medicine & Biology* **47** 3789

Chapter 3. Reusable Biosensor – Fluorescence Biosensor and FET based Biosensor

3.1. Introduction

Biosensors are a key component for versatile analytical applications such as disease diagnosis [1-9], drug screening [10], environmental monitoring [11], and bioterrorism prevention [12]. Until now, most of conventional biosensors have been manufactured as a disposable chip only for a one-time use. However, for various applications, one needs to use a single biosensor chip for repeated sensing operations. For example, recent progress of nano-biotechnology enabled various advanced nano-biosensors such as carbon nanotube (CNT) transistor-based biosensors [13], nanowire-based biosensors [14], and magnetic beads-based biosensors [15], Such nano-biosensors take an advantage of the superior characteristics of nano-devices [16] exhibit high performances such as a high sensitivity and a fast response time. However, one of the major hurdles holding back their practical applications can be a rather high cost of such nano-devices [17], Thus, a strategy to reuse a single nano-biosensor chip for repeated sensing operations can be a key stepping stone to bring such high-performance, but expensive, nano-biosensors toward practical applications. On the other hand, there have been extensive efforts to develop an alarming system which can be installed in a public place (e.g. airport) and used to monitor hazardous viruses or bioterror substances in the air for a long time period [18, 19]. For such applications, one needs a reusable biosensor device which can be utilized repeatedly over a long time period without being replaced. Extensive efforts have been given to develop reusable nano-biosensor chips

using various methods such as chemical refreshment of receptors, magnetic bead-based methods etc [20-26]. However, previous methods often leave chemical contaminations or thick layers of receptors on sensor chip surfaces, limiting their applications only for some specific receptor molecules or sensor structures.

Herein, we report a magnetically-refreshable receptor platform (MRP) structure which can be integrated with virtually-general nano-biosensor structures to build *reusable* nano-biosensor chips. The hysteresis properties of ferromagnetic MRP structures integrated with a nano-biosensor were utilized to generate *attractive* or *repulsive* forces between receptor-functionalized magnetic nanobeads and the ferromagnetic MRP structures under external magnetic fields, so that one can *trap* or *remove* receptors on the nano-biosensor, respectively. Thus, one can easily remove used receptor molecules on the nano-biosensor surface and place new receptors with a controlled thickness for repeated sensing operations. Furthermore, since the residual magnetization of the ferromagnetic MRP structures can hold receptor-functionalized nanobeads on the sensor surfaces without external magnetic fields, the sensors can be used for versatile applications such as imaging analyses and sensing operations in a conventional manner without external magnetic fields. The MRP structure was successfully utilized to build reusable immunofluorescence biosensor chips for repeated sensing operations while maintaining its sensitivity and selectivity. Significantly, since, in this method, receptor-functionalized nanoparticles form single-

layered film structures without stacking as multiple layers on the MRP structures, one can place receptors close to the nano-biosensor surfaces. Note that some nano-biosensor structures such as transistor-based electrical biosensors require receptor molecules close to sensor surfaces for sensing operations. We successfully integrated the MRP structures with CNT transistor structures to build reusable biosensor chips. The MRP structure is a simple but versatile structure which can be applied for quite versatile nano-biosensor structures and virtually-general receptor molecules to build reusable biosensor chips. Thus, it can be a major breakthrough which can bring rather expensive nano-biosensors for practical applications and may even enable new bio-analysis applications such as monitoring of hazardous biological entities in public places.

3.2. Experimental methods

3.2.1 Preparation of antibody-functionalized nanobeads, fluorescence-labeled capture antibody, and antigens.

Human interleukins (IL-4, IL-10), their biotinylated detection antibody (labeled as 1^{st} antibody), capture antibody (labeled as 2^{nd} antibody) and an antigen were purchased from eBioscience company (USA). Streptavidin-coated pink-fluorescent superparamagnetic nanobeads (Nano-screenMAG-Streptavidin, with its hydrodynamic diameter of 100 nm, 1 mg/mL in PBS solution) were purchased from Chemicell GmbH (Germany). Fluorescein isothiocyanate (FITC), Poly(ethylene glycol) thiol (PEG-SH, MW 5000)

and other chemical reagents were purchased from Sigma-Aldrich (USA). To prepare nanobeads functionalized with 1st antibody, 100 μL solution of the streptavidin-coated superparamagnetic nanobeads (1 mg/mL in PBS solution) was first mixed with 20 μL solution of the biotinylated 1st antibody (1 mg/mL in PBS solution), and the mixed solution was incubated at room temperature for 1 hour. Finally, it was diluted to 1000 μL in PBS solution. The conjugation of 2nd antibody with FITC was performed following the procedure of the FluoroTag FITC conjugation kit.

3.2.2. Experimental procedure for trapping and detrapping of single-layered film structures of fluorescence-labeled nanobeads.

A solenoid (custom made, NS Magnet, Korea) was purchased and used for generating external magnetic fields. The solenoid was comprised of 7500 turned electric wires and a 1.5 cm × 6.3 cm cylindrical iron core. For the trapping of fluorescence-labeled nanobeads as a single-layered film structure, 50 μL (1 mg/mL in PBS solution) of fluorescence-labeled magnetic nanobead solution was placed on MRP structures patterned on a SiO_2 substrate, and an external magnetic field (150 mT) was applied in a perpendicular direction to the substrate for 90 seconds. After removing the magnetic field, the substrate was washed by PBS solution. For the detrapping of the nanobeads, 35 mT of an external magnetic field in an opposite direction was applied for 10 seconds, and the substrate was washed by PBS solution. After each trapping and detrapping steps, the amount of

the fluorescence-labeled nanobeads assembled on the substrate was measured by a fluorescence microscope (TE2000U, Nikon, Japan) with a rhodamine filter.

3.2.3. Fabrication of reusable fluorescence biosensors.

Ferromagnetic MRP patterns (10 nm Au on 10 nm Ni, 30 × 28 Ni/Au patterns of size 4 μm × 8 μm) were fabricated on a SiO_2 substrate (100 nm-thick SiO_2 film on Si wafer) via conventional microfabrication processes. The substrate with the patterns was immersed in an octadecyltrichlorosilane (OTS) solution (1:500, v/v in hexane) for 5 minutes and then rinsed thoroughly by anhydrous hexane. Here, a self-assembled OTS monolayer formed on SiO_2 surface passivated the SiO_2 surfaces. Later, the substrate was immersed in a PEG-SH solution (20 mg/mL in deionized water) for ~10 hours at room temperature. In this process, PEG layer was formed on the Au film over the ferromagnetic nickel-based MRP structures, which minimized the adhesion of biomolecules and nanobeads on the MRP structures.

3.2.4. Repeated sensing operations of reusable fluorescence biosensors.

50 μL solution of antibody-functionalized magnetic nanobeads was first placed on a SiO_2 substrate with ferromagnetic MRP structures, and an external magnetic field (150 mT) was applied in a perpendicular direction to the substrate plane for 90 seconds. In this step, a monolayer of antibody-functionalized nanobeads was assembled on the ferromagnetic MRP

structures so that the antibody molecules on the nanobeads can be utilized for a biosensing operation. The assembly of nanobeads was confirmed by observing the fluorescence from the nanobeads via a fluorescence microscope. For a complementary sensing operation, the 50 μL solution of a complementary antigen (1 ng/mL ≈ 57.1 pM in PBS solution) was placed on the substrate with assembled nanobeads for 1 hour at room temperature and then washed thoroughly with PBS solution. Subsequently, the substrate was incubated with FITC-2nd antibody at room temperature for 1 hour. Finally, the selective detection of the antigen was confirmed by observing the fluorescence from FITC-2nd antibodies on the ferromagnetic MRP structures via a fluorescence microscope. After one sensing operation, 35 mT of an external magnetic field was applied in an opposite direction for 10 seconds, which removed the magnetic nanobeads from the MRP structures. Following this, the solution on the substrate was washed away with clean PBS solution, leaving clean substrate surfaces for additional sensing operations.

3.2.5. Fabrication of reusable carbon nanotube-based electrical biosensors with ferromagnetic MRP structures.

Purified semiconducting single-walled carbon nanotubes (swCNT) were purchased from NanoIntegris Inc. (USA) and used as received. The CNTs had a diameter of 0.7-2 nm and a length of 2-3 μm. A CNT transistor with floating electrodes could be fabricated following the method reported

previously [27]. At first, "surface-programmed assembly" method was used to pattern swCNT network channels on a SiO_2 substrate. Briefly, the patterns of photoresist layer (AZ5214) were first prepared on the SiO_2 substrate via conventional photolithography, and the substrate was placed in the solution of OTS (1:500, v/v in hexane) for 5 minutes at room temperature so that the self-assembled monolayer (SAM) of OTS was formed on the bare SiO_2 surface. Later, substrate was rinsed with clean anhydrous hexane, acetone, and ethanol in sequence, leaving OTS SAM patterns and bare SiO_2 surface regions. The substrate is placed in the CNT solution (0.1 mg/mL in 1,2-dichlorobenzene) for 30 seconds so that CNTs in the solution were selectively adsorbed onto the bare SiO_2 surface regions and formed CNT network channels. The wafer was rinsed thoroughly with 1,2-dichlorobenzene and dried with nitrogen gas. In this work, we prepared swCNT channels with its width of 3 μm. The source and drain electrodes (30 nm Au on 10 nm Ti), and the five floating electrodes (10 nm Au on 10 nm Ni) were fabricated via conventional photolithography, thermal evaporation, and lift-off processes. Following this, the source and drain electrodes were covered with a photoresist layer (DNR-L300-30) to passivate the electrodes. The fabricated devices were immersed in the PEG-SH solution (20 mg/mL in deionized water) for overnight and washed with deionized water so that PEG layer was formed on the floating electrodes and minimized the non-specific adsorption of biomolecules during biosensing experiments. The devices were also immersed in the TWEEN-20 solution

(0.5%) for 10 minutes and washed by deionized water to passivate the CNT channel surface [27].

3.2.6. Repeated sensing operations of reusable carbon nanotube transistor-based biosensors.

The bio-sensing operations of reusable CNT based biosensors were performed in PBS solution using an Ag/AgCl electrode as a liquid gate electrode. At first, the solution of antibody-functionalized nanobeads (1 mg/ml in PBS solution) was applied to the CNT device, and an external magnetic field (150 mT) was applied along the vertical direction to the substrate surface for 90 seconds so that a monolayer of nanobeads were assembled on the surface of ferromagnetic MRP structure in the floating electrodes. Afterwards, target molecular solution was applied to the device while monitoring the source-drain current with a source-drain bias of 100 mV and liquid gate bias of -200 mV. The source-drain currents of CNT transistor devices were measured using a semiconductor characterization system (4200-SCS, Keithley, USA). The current change ratio $\Delta I / I_0$ was utilized as a sensing signal.

3.2.7. Morphological analysis.

AFM imaging was performed using a commercial AFM system (MFP-3D, Asylum Research) in a tapping mode. A field emission scanning electron

microscope (FE-SEM) (Hitachi 4800, Hitachi) was used for the SEM imaging.

3.3. Repeated Sensing Operation of a Reusable Nano-biosensor based on a MRP Structure

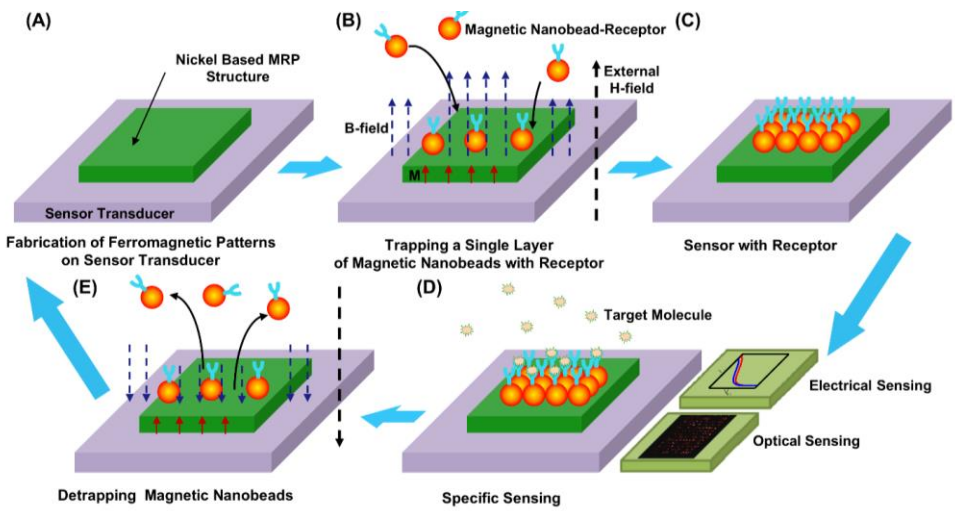

Figure 3-1. Schematic diagram showing the repeated sensing operations of a reusable nano-biosensor based on a MRP structure. (A) Fabrication of a ferromagnetic MRP structure on a biosensor transducer surface. (B) Trapping of single-layered film structures of magnetic nanobeads functionalized with receptors via a rather strong external magnetic field. A *black dashed arrow*, *red arrows*, and *blue dashed arrows* represent *an external magnetic field*, *the magnetization of the ferromagnetic MRP structure*, and *total magnetic fields*, respectively. (C) Formation of a single-layered film structure of magnetic nanobeads on the ferromagnetic MRP structure. (D) Sensing operation using the receptor molecules on the assembled nanobeads. (E) Removal of the nanobeads.

Figure 3-1 shows the schematic diagram showing the repeated sensing operations of a biosensor based on a ferromagnetic MRP structure. Detailed processes are presented in the Experimental Methods Section. In brief, a MRP structure based on ferromagnetic nickel thin film patterns were first fabricated as a part of a biosensor device in the active sensing regions of the biosensor device so that the biosensor can respond to the binding activity of the receptors in the regions (Figure 3-1A). Depending on the biosensor structures, the ferromagnetic MRP structures can be integrated in different formations. For example, in case of transistor-based electrical sensors, the MRP structures can be a part of its electrodes. For a sensing operation, the biosensor was placed in the solution of magnetic nanobeads (orange spheres) functionalized with specific receptor molecules (y-shaped symbols), and external magnetic fields (black dashed arrows) were applied in a perpendicular direction to the MRP structures (Figure 3-1B). In the external magnetic fields, the ferromagnetic MRP structures were magnetized (red arrows) along the direction of the external fields, and the magnetic fields (blue dashed arrows) just above the pattern became stronger than those in other regions. Thus, the magnetic nanobeads in the solution were attracted toward the MRP structures and formed a layered structure. Here, using ferromagnetic MRP structures with a proper thickness and shape, we could generate strong

magnetic field regions only in a very short distance above the structures so that nanobeads formed a single-layered film structure (Figure 3-1C). Note that the residual magnetization of the ferromagnetic MRP structures can hold assembled magnetic nanobeads even without any external magnetic fields. Thus, we could take out the MRP structures from the solution environments with external magnetic fields and perform sensing operations in a conventional manner without any external magnetic fields. Since the receptors on the assembled nanobeads were near the biosensor surface, they can be utilized for the selective detection of specific target molecules via the biosensor (Figure 3-1D). As a proof of concepts, we demonstrated the repeated sensing operations of biosensors based on fluorescence and carbon nanotube transistor measurements. After the sensing operation, a rather weak external magnetic fields with a reversed direction was applied *so that the magnetic fields in the solution was reversed while the magnetization of the MRP structures remained* due to the hysteresis of the ferromagnetic materials (Figure 3-1E). In this case, since the remaining magnetization of the ferromagnetic MRP structures had an opposite direction to the external magnetic fields, total magnetic fields just above the MRP structures became weaker than those in other regions. Thus, the magnetic nanobeads were moved away from the MRP structures, and the surface of the sensor transducer was restored to a clean surface (Figure 3-1A).

By repeating these processes, we could perform repeated sensing operations using a single biosensor chip. Importantly, since our method relies only on physical forces without any chemical treatment to refresh used receptor molecules, one can minimize possible contaminations and it can be applied for virtually-general receptor species. Furthermore, in our process, the magnetic nanobeads formed a single-layered film structure on the transducer surface, which allows one to apply our method to versatile biosensor devices including those which require receptors close to biosensor surfaces.

3.4. Single-layer Trap and Release of Magnetic Particles on a MRP Structure

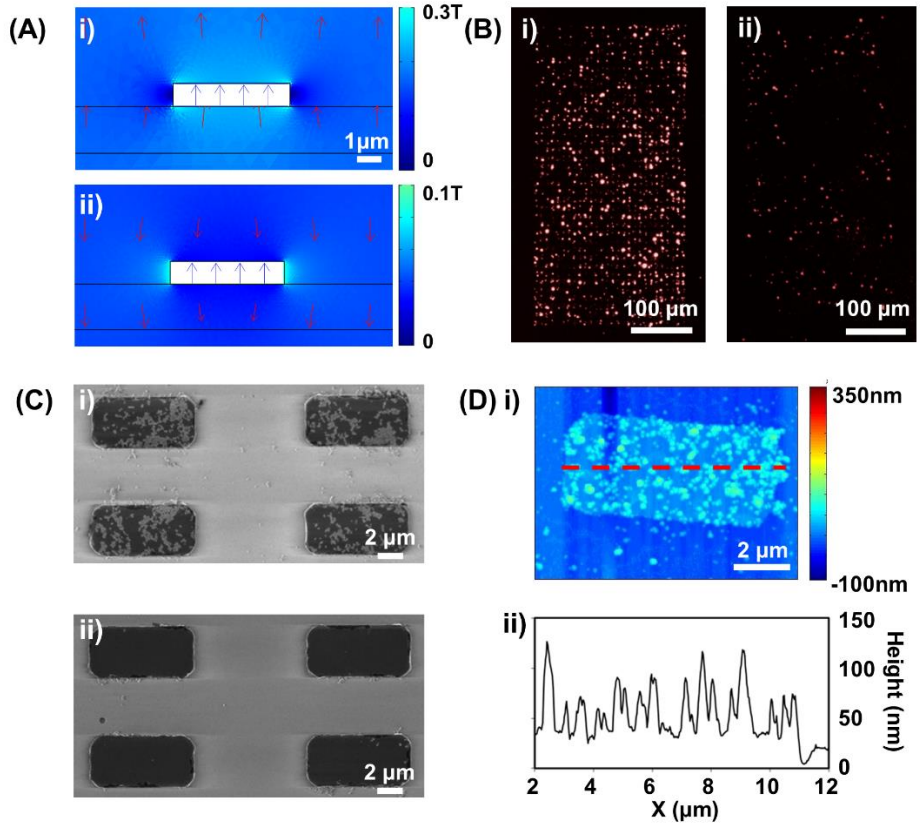

Figure 3-2. Trapping and detrapping of magnetic nanobeads on MRP structures. (A) Simulation results showing the cross-sectional view of a magnetic field strength around a MRP structure during i) trapping and ii) detrapping steps. *Brighter blue regions* and a *rectangle* represent the regions with *a stronger magnetic field* and a *MRP structure*, respectively. *Red* and *blue* arrows indicate the direction of the *magnetic fields* and the *magnetization of the MRP structure*, respectively. (B) Fluorescence images of MRP structures after i) trapping and ii) detrapping of fluorescence–labeled magnetic nanobeads. (C) SEM images of ferromagnetic MRP

structures after i) trapping and ii) detrapping magnetic nanobeads. *Black rectangles and small gray circles* represent ferromagnetic *MRP structures* and *trapped magnetic nanobeads*, respectively. (D) i) AFM image of a MRP structures (rectangular bright region) after trapping magnetic nanobeads (small white dots) and ii) height profiles along the dashed line in i).

Figure 3-2A depicts the simulation results showing magnetic field strength around a nickel-based MRP structure when external magnetic fields were applied during the trapping and detrapping steps. Here, the simulation was performed using COMSOL multiphysics software. When a *strong* external magnetic field was applied with an upward direction, the MRP structure was magnetized along the external magnetic field direction [Figure 3-2A(i)]. In this case, the magnetic field by the magnetized MRP structure was added to the external magnetic field in the region just above the structure, resulting in a stronger magnetic field [brighter regions in Figure 3-2A(i)] than that in other regions. Thus, we can expect that nearby superparamagnetic nanobeads can be attracted toward the MRP structure because magnetic dipoles are driven to the regions with a stronger magnetic field. Significantly, such a stronger magnetic field region extended only in a very short distance from the MRP structure, which may enable the assembly of single-layered structures of the nanobeads. On

the other hand, when a rather *weak* external magnetic field with a *reversed* direction was applied, the magnetization remained because of the magnetic hysteresis of the nickel-based MRP structure [Figure 3-2A(ii)]. In this case, the magnetic field by the MRP structure had an opposite direction to that of the external magnetic field, and, thus, the magnetic field just above the MRP structure became *weaker* [darker regions in Figure 3-2A(i)] than in other regions. Here, we can expect any superparamagnetic nanobeads on the MRP structure are moved away from the structure. These simulation results indicate that the hysteresis properties of ferromagnetic nickel-based MRP structures with a proper dimension can be utilized to exert *attractive* or *repulsive* forces to *trap* or *detrap* a precise amount of receptor-functionalized nanobeads down to a single-layer precision, respectively.

Figure 3-2B *(i)* and *(ii)* show the fluorescence images of the 30 × 28 array of nickel-based MRP structures after the *trapping* and *detrapping* of fluorescence-labeled magnetic nanobeads, respectively. The detailed procedure for trapping of the single-layered structures of nanobeads is presented in the Experimental Methods section. For the trapping of nanobeads, the external magnetic fields of 150 mT was applied in the direction perpendicular to the substrate surface. The fluorescence image shows well-ordered bright spots corresponding to the array of MRP structures, indicating high yield of the magnetic trapping process [Figure 3-2B(i)]. For the detrapping process, rather

weak magnetic fields of 35 mT in the reversed direction was applied, and the solution on the substrate was replaced with PBS solution. The result shows that most of nanobeads were removed from the substrate [Figure 3-2B(ii)], indicating that the detrappng process can efficiently remove the nanobeads from the substrate. These results indicate our method can be utilized to trap and detrap nanobeads over a large surface area with a high efficiency in real-time, which can be critical for practical applications. It also should be noted that this process can be performed without any chemical treatment, implying our method should be compatible with most of receptor molecules for various biosensing applications.

Figure 3-2C *(i)* and *(ii)* show the field emission scanning electron microscope (SEM) images displaying the ferromagnetic nickel-based MRP structures (dark rectangular area) with nanobeads (white circular dots) after *trapping* and *detrapping* processes, respectively. After trapping and washing steps, magnetic nanobeads were found to form single-layered film structures on the MRP structures without being aggregated or stacked in a vertical direction [Figure 3-2C(i)]. Note that due to the residual magnetization of the ferromagnetic MRP structures, the magnetic nanobeads remained on the sensor surface even after removing external magnetic fields and washing the surface. Thus, one can take out the sensors with assembled nanobeads from the solution and use them for quite versatile applications and analyses such as SEM imaging and conventional

sensing operations without external magnetic fields. The SEM images of assembled magnetic nanobeads after washing steps were analyzed to estimate the working area including the magnetic beads on the MRP structures, resulting in the working area value of ~31% out of the entire MRP structure surface (Supplementary Data). Furthermore, from the surface area of a MRP structure and the measured number of antibody molecules on individual nanobeads, we can estimate that the number of antibody molecules on each MRP structure was ~ 6.7×10^4 (Supplementary Data). After the detrapping process, most of the magnetic nanobeads were removed from the MRP structures, indicating the high efficiency of our trapping-detrapping method [Figure 3-2C(ii)].

To confirm the formation of single-layered structures of nanobeads, the atomic force microscopy (AFM) characterization was performed (Figure 3-2D). The AFM topography image shows that most of nanobeads were trapped on the MRP structures and formed a layer with a rather uniform height [Figure 3-2D(i)]. The height profile along the red dashed line in the topography shows the height of the trapped nanobeads up to 50 nm, which corresponds to the hydrodynamic diameter of ~100 nm [Figure 3-2D(ii)] [28]. It supports that the trapped nanobeads formed a monolayer structure without aggregation.

3.5. Reusable Immunofluorescence Biosensors

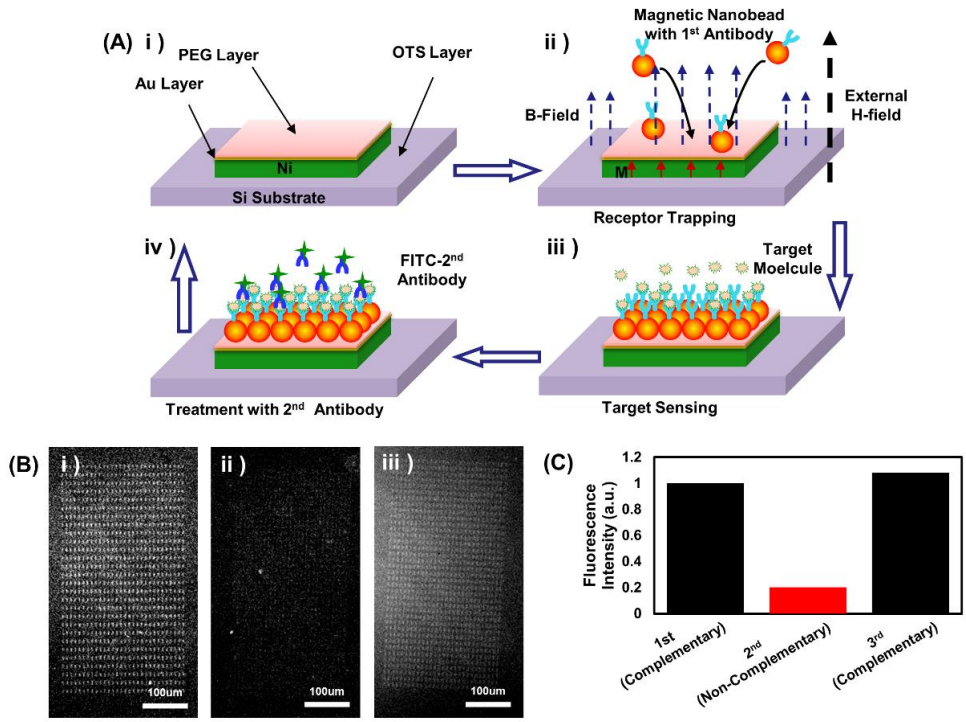

Figure 3-3. Reusable immunofluorescence sensors based on MRP structures. (A) A schematic diagram showing the repeated sensing operation of a fluorescence sensor based on the MRP structures. (B) i) Fluorescence images after the first sensing test with IL-4 target molecules and corresponding *complementary* antibodies, ii) the second sensing test with the same antibodies and *non-complementary* IL-10 target molecules, and iii) the third sensing test with the same antibodies and the *complementary* IL-4 target molecules. Bright regions represent those with the IL-4 2nd antibody conjugated with fluorescent FITC dye. (C) Fluorescence intensity measured from the fluorescence images in (B).

Figure 3A displays the operation of reusable fluorescence biosensors based on the MRP structures. Detailed processes are shown in the Experimental Methods section. In brief, ferromagnetic nickel-based MRP structures passivated with PEG layer were fabricated via conventional microfabrication processes [Figure 3A(i)]. Here, the thin Au layer provided a stable surface without oxidation and, thus, enabled good interface with biological solution, which can be very important for the sensing operation of some electrical sensors such as carbon nanotube transistor-based electrical sensors. Furthermore, as a part of the fabrication process, we could apply well-known thiol chemistry to coat the Au surface with passivation molecules such as PEG, which prevented unwanted non-specific adsorption of biomolecules during the sensing operations. For a sensing operation, magnetic nanobeads functionalized with the 1^{st} antibody were first assembled on the MRP structures by a rather strong magnetic field [Figure 3-3A(ii)]. After that, target molecular species was applied so that target molecules could selectively bind to the complementary antibody on the nanobeads assembled on the ferromagnetic MRP structures [Figure 3-3A(iii)]. Finally, the 2^{nd} antibody labeled with fluorescein isothiocyanate (FITC) was applied to the sensor, and the fluorescence from the 2^{nd} antibody bound on the sensor surface was measured using a fluorescence microscope to confirm the selective

sensing of target molecular species [Figure 3-3A(iv)]. After entire sensing processes, a rather weak magnetic field with a reversed direction was applied to remove the magnetic nanobeads, leaving clean sensor surface for additional sensing operations. Note that since this process does not require any chemical process to refresh used sensors, it can be applied to virtually-general receptors for versatile biosensing applications.

Figure 3-3B shows the fluorescence images of three consecutive sensing experiments repeating the processes in Figure 3-3A. For the first complementary sensing experiment, nanobeads functionalized with the 1st antibody for IL-4 were assembled on the array of ferromagnetic MRP structures, and then a complementary target protein (IL-4, 57.1 pM in PBS solution) followed by the fluorescence-labeled complementary 2nd antibody were applied [Figure 3-3B(i)]. Note that the fluorescence image shows the array of fluorescent spots corresponding to the array of ferromagnetic structures, indicating the selective binding of complementary target molecules as well as fluorescence-labeled 2nd antibody. This result clearly shows that the antibody molecules assembled onto the ferromagnetic MRP structures were working properly, and they can be utilized for selective biosensing applications. After the first experiment, the nanobeads were removed by applying a rather weak magnetic field with a reversed direction, and the *second* experiment with the same antibody for IL-4

and *non-complementary* target molecules (IL-10, 67.6 pM in PBS solution) were performed, resulting in low fluorescence signals [Figure 3-3B(ii)]. It indicates the non-specific reaction in our sensor was very small. Furthermore, it also should be noted that the fluorescence signals in the first experiment [Figure 3-3B(i)] actually came from the *fluorescence-labeled 2nd antibody bound to 1st antibody with the complementary targets on the sensor surface*. Thus, the low fluorescence intensity after the second sensing experiment [Figure 3-3B(ii)] implies the efficient removal of the antibodies used for the first experiment. After removing nanoparticles again, we performed the *third* experiment with the same antibodies and *complementary* targets (IL-4, 57.1 pM in PBS solution) on the same chip [Figure 3-3B (iii)]. Note that we can achieve the selective detection of target molecules again. These results clearly show that we can remove used receptors and repeatedly use a single chip for multiple sensing operations.

Figure 3-3C shows the graph of fluorescence intensity resulting from each sensing experiment. Note that the second sensing result using non-complementary target molecules exhibited quite a low fluorescence intensity, which means that the magnetic beads and their attached FITC molecules used in the first experiment were removed, and the non-complementary target molecule was not attached to the 1st antibody. On the other hands, the fluorescence intensity as a result of the third experiment using complementary target molecules recovered

back to high intensity like that of the first complementary sensing experiment. These results clearly show that the reusable fluorescence sensors based on our MRP structure can be utilized repeatedly while maintaining its high selectivity and sensitivity.

3.6. Reusable CNT-FET Biosensors

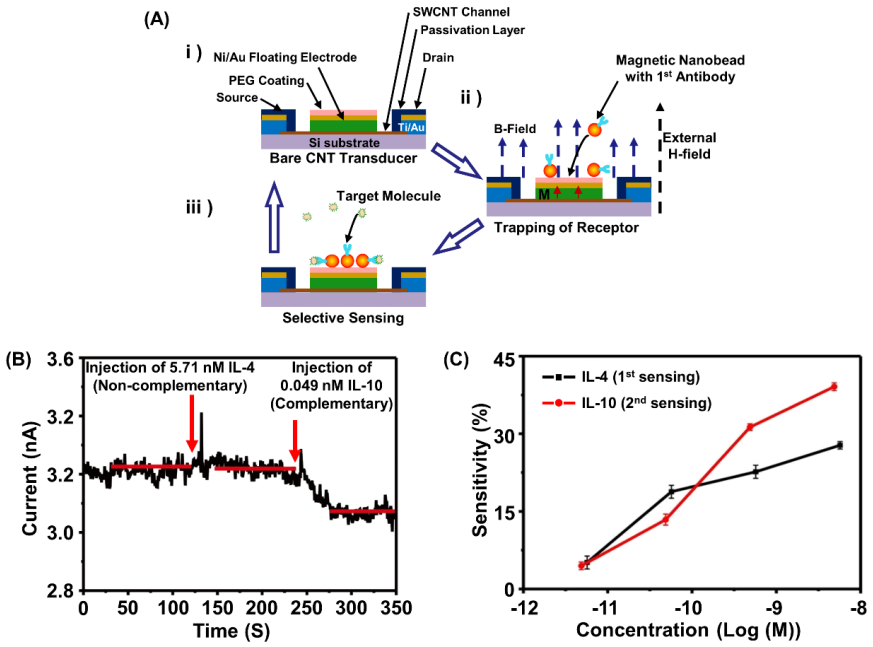

Figure 3-4. Reusable CNT transistor-based biosensors based on MRP structures. (A) A schematic diagram showing the repeated sensing cycle of a reusable CNT transistor-based electrical biosensor; (i) CNT transistor comprised of CNT network channels between source and drain electrodes with fixed bias voltages and floating electrodes based on Ni, (ii) assembly of nanobeads functionalized with 1st antibody onto the floating electrodes via external magnetic fields, (iii) sensing of target molecules. (B) Real-time sensor responses after the introduction of IL-4 and IL-10 target proteins to a CNT transistor-based sensor including assembled nanobeads functionalized with IL-10 antibody. (C) Sensing of two different target molecules (IL-4

and IL-10) by repeating the sensing experiments using nanobeads functionalized with corresponding two different antibodies.

Figure 3-4A illustrates the schematic diagram for the repeated sensing operations of a reusable CNT transistor-based electrical biosensor. The detailed procedure is presented in the Experimental Methods section. In brief, a CNT transistor device with floating electrodes was first fabricated as reported previously [Figure 3-4A(i)] [27]. This device is comprised of CNT network channel connecting source and drain electrodes with fixed bias voltage and floating electrodes in the middle of the CNT channel. Here, the MRP structure based on nickel was integrated as a part of the floating electrode. In this sensor, the selective binding of biomolecules to receptor molecules on the floating electrode surface altered the work function of the Au electrode and, eventually, changed the electrical currents in the CNT transistor. Thus, one can detect the target molecules simply by monitoring the electrical current change in the transistor device. Note that since this CNT transistor-based sensor responds to target molecules only within the Debye length distance from the floating electrode surface, it is critical to place the receptor molecules close to the electrode surface. For a sensing operation, the solution of 1st antibody-functionalized nanobeads was applied to the CNT transistor, and an external magnetic field was applied so that the nanobeads in the solution were assembled on the floating electrodes with the nickel-based MRP structure [Figure 3-4A(ii)]. After trapping nanobeads, the

magnetic field was removed so that it does not disturb the CNT transistor during the sensing operations. Note that due to the residual magnetization of ferromagnetic MRP structures, the magnetic nanobeads remained on the sensor surface even after removing external magnetic fields. It should be mentioned that in previous methods using only external magnetic fields without ferromagnetic patterns, rather strong external magnetic fields were usually required to hold stable amounts of magnetic beads on the sensor surface, which could generate electrical noises and disturb the operation of highly-sensitive nano-biosensors [20, 24]. When the solution of target molecules was applied, the target molecules selectively bound to the antibody on the assembled nanobeads and, eventually, altered the electrical currents in the CNT transistor device, which was utilized as a sensing signal [Figure 3-4A(iii)]. Significantly, in our method, nanobeads formed a single-layered structure on the floating electrodes so that antibody molecules on the assemble nanobeads were within a Debye length from the electrode surface and the sensor can detect the selective binding of target molecules onto the receptor molecules. After the sensing step, the nanobeads can be removed simply by applying a rather weak magnetic field with a reversed direction, leaving clean floating electrode surface for additional sensing operations. It should be mentioned that since the used antibody on the sensor surface can be refreshed simply by adjusting external magnetic fields without relying on chemical processes, this process can be applied for versatile sensors based on virtually-general receptor molecular species.

Figure 3-4B shows the real-time response of a reusable CNT transistor-based sensor based on MRP structures by the addition of non-complementary (IL-4) and complementary (IL-10) biomolecular species. Here, nanobeads with IL-10 antibody were first trapped on the Ni/Au floating electrode surface, and a 5.71 nM of non-complementary biomolecular (IL-4) solution and a 0.049 nM of complementary biomolecular (IL-10) solution were applied in sequence while monitoring the electrical currents between source and drain electrodes. Note that the electrical currents did not change by the addition of non-complementary IL-4 molecules, while the addition of the complementary IL-10 molecular species resulted in the clear change of electrical currents. This result clearly shows that the receptors on the trapped nanobeads functioned properly, and our sensors selectively detect the target molecules. Previous works show that some biosensors such as transistor-type or surface plasmon resonance-based biosensors can detect target molecules only within a short distance from the device surface [25, 26]. Since, in our method, the nanobeads with receptors formed a single-layered structure on our device surface, the receptors can be place within a short distance from the device surface, enabling the sensing operation of such sensors. Thus, the formation of single-layered film structures of nanobeads in our method can be a significant advantage in building reusable sensors based on such sensor transducer devices [27, 29].

Since our method allows one to repeatedly functionalize and refresh

receptor molecules on a device surface, we could easily functionalize a single CNT transistor device with different receptor molecules and use it to detect different target molecules (Figure 3-4C). In this experiments, nanobeads with IL-4 antibody were first assembled on a CNT transistor device, and the device was utilized to detect IL-4 with different concentrations from 100 pg/mL to 100 ng/mL (black dots in Figure 3-4C). The nanobeads with used antibody could be removed by applying external magnetic fields with a reversed direction. Later, nanobeads functionalized with IL-10 antibody were assembled again onto the floating electrode surface, and the sensing experiment using IL-10 molecular solution was performed (red dots in Figure 3-4C). The results show the increasing response of our sensors with increasing target molecular concentrations. The graphs were fitted using the equation based on Langmuir isotherm model as reported previously [27]. From the fitting, we can estimate the equilibrium constant of *IL-4* and *IL-10* as $3.36 \times 10^{10}\ M^{-1}$ and $5.08 \times 10^{10}\ M^{-1}$, respectively. These values are in the same order as those reported previously [30]. These results show that our MRP structure allowed one to use a single transducer device for the detection of different molecular species, which clearly shows the versatility and effectiveness of our method.

3.7. Summary

In conclusion, we developed the MRP structure which can be integrated with versatile nanodevice-based sensor transducers to build reusable

biosensors based on virtually-general receptor molecules. The magnetic hysteresis properties of the ferromagnetic MRP structures integrated as a part of a nano-biosensor were utilized to trap or remove magnetic nanobeads with receptor molecules on the nano-biosensor device for repeated sensing operations. Using the MRP structure, we demonstrated the repeated sensing operations of fluorescence biosensors and CNT transistor-based electrical biosensors. Significantly, since entire multiple biosensing operations can be done simply by adjusting external magnetic fields without using any harsh chemical treatment, this MRP structure can be applied to versatile biosensors based on virtually-general receptor molecules. Furthermore, this method allows one to assemble a single-layered film structure of receptor-functionalized nanobeads on the biosensor surface so that active antibody can be placed within a very short distance from the biosensor surface. Thus, this MRP structure can be utilized for some biosensors (e.g. transistor-type, SPR-based) which require receptor molecules very close to the sensor surface. We also demonstrated the detection of two different target molecular species using only a single CNT transistor-based biosensor chip. Our method is a simple but powerful strategy which allows one to reuse rather expensive nano-biosensor devices and, eventually, bring them for practical applications. In addition, it may give the way toward advanced biosensing applications such as a real-time monitoring system of hazardous viruses in public places.

3.8. References

[1] Hansen J A, Sumbayev V V and Gothelf K V 2007 An Electrochemical Sensor Based on the Human Estrogen Receptor Ligand Binding Domain *Nano Lett.* **7** 2831-4

[2] Ko J W, Woo J-M, Jinhong A, Cheon J H, Lim J H, Kim S H, Chun H, Kim E and Park Y J 2011 Multi-Order Dynamic Range DNA Sensor Using a Gold Decorated SWCNT Random Network *ACS Nano* **5** 4365-72

[3] Inci F, Tokel O, Wang S, Gurkan U A, Tasoglu S, Kuritzkes D R and Demirci U 2013 Nanoplasmonic Quantitative Detection of Intact Viruses from Unprocessed Whole Blood *ACS Nano* **7** 4733-45

[4] Farrow B, Hong S A, Romero E C, Lai B, Coppock M B, Deyle K M, Finch A S, Stratis-Cullum D N, Agnew H D, Yang S and Heath J R 2013 A Chemically Synthesized Capture Agent Enables the Selective, Sensitive, and Robust Electrochemical Detection of Anthrax Protective Antigen *ACS Nano* **7** 9452-60

[5] Lo Y-S, Nam D H, So H-M, Chang H, Kim J-J, Kim Y H and Lee J-O 2009 Oriented Immobilization of Antibody Fragments on Ni-Decorated Single-Walled Carbon Nanotube Devices *ACS Nano* **3** 3649-55

[6] Zhang T, He Y, Wei J and Que L 2012 Nanostructured optical microchips for cancer biomarker detection *Biosens. Bioelectron.* **38** 382-8

[7] Alwarappan S, Erdem A, Liu C and Li C-Z 2009 Probing the Electrochemical Properties of Graphene Nanosheets for Biosensing Applications *The Journal of Physical Chemistry C* **113** 8853-7

[8] Alwarappan S, Liu G and Li C-Z Simultaneous detection of dopamine, ascorbic acid, and uric acid at electrochemically pretreated carbon nanotube biosensors *Nanomed. Nanotechnol. Biol. Med.* **6** 52-7

[9] Mishra M, Alwarappan S, Joshi R K and Mohanty T 2013 Chemically Synthesized Graphene for Electrochemical Biosensing *Journal of Nanoscience and Nanotechnology* **13** 4040-4

[10] Liu Y, Yu X, Zhao R, Shangguan D-H, Bo Z and Liu G 2003 Quartz crystal biosensor for real-time monitoring of molecular recognition between protein and small molecular medicinal agents *Biosens. Bioelectron.* **19** 9-19

[11] An J H, Park S J, Kwon O S, Bae J and Jang J 2013 High-Performance Flexible Graphene Aptasensor for Mercury Detection in Mussels *ACS Nano* **7** 10563-71

[12] Radke S M and Alocilja E C 2005 A microfabricated biosensor for detecting foodborne bioterrorism agents *Sensors Journal, IEEE* **5** 744-50

[13] Chen X, Kim D and Hong S 2014 The carbon nanotube-based nanobiosensor: a key component for ubiquitous real-time bioscreening system? *Nanomedicine* **9** 565-7
[14] Yeh P-H, Li Z and Wang Z L 2009 Schottky-Gated Probe-Free ZnO Nanowire Biosensor *Adv. Mater.* **21** 4975-8
[15] Baselt D R, Lee G U, Natesan M, Metzger S W, Sheehan P E and Colton R J 1998 A biosensor based on magnetoresistance technology1 *Biosens. Bioelectron.* **13** 731-9
[16] Sosa N E, Chen C, Liu J, Xie S, Marks T J and Hersam M C 2010 Nanoscale Structure, Composition, and Charge Transport Analysis of Transparent Conducting Oxide Nanowires Written by Focused Ion Beam Implantation *J. Am. Chem. Soc.* **132** 7347-54
[17] Li W-S, Hou P-X, Liu C, Sun D-M, Yuan J, Zhao S-Y, Yin L-C, Cong H and Cheng H-M 2013 High-Quality, Highly Concentrated Semiconducting Single-Wall Carbon Nanotubes for Use in Field Effect Transistors and Biosensors *ACS Nano* **7** 6831-9
[18] Sapsford K E, Shubin Y S, Delehanty J B, Golden J P, Taitt C R, Shriver-Lake L C and Ligler F S 2004 Fluorescence-based array biosensors for detection of biohazards *J. Appl. Microbiol.* **96** 47-58
[19] Asada H H, Shaltis P, Reisner A, Sokwoo R and Hutchinson R C 2003 Mobile monitoring with wearable photoplethysmographic biosensors *IEEE Eng. Med. Biol. Mag.* **22** 28-40
[20] Sun Y, Bai Y, Song D, Li X, Wang L and Zhang H 2007 Design and performances of immunoassay based on SPR biosensor with magnetic microbeads *Biosens. Bioelectron.* **23** 473-8
[21] Wang D, Chen G, Wang H, Tang W, Pan W, Li N and Liu F 2013 A reusable quartz crystal microbalance biosensor for highly specific detection of single-base DNA mutation *Biosens. Bioelectron.* **48** 276-80
[22] Gijs M M 2004 Magnetic bead handling on-chip: new opportunities for analytical applications *Microfluid. Nanofluid.* **1** 22-40
[23] Xu Y and Wang E 2012 Electrochemical biosensors based on magnetic micro/nano particles *Electrochim. Acta* **84** 62-73
[24] Zhu D, Liu J, Tang Y and Xing D 2010 A reusable DNA biosensor for the detection of genetically modified organism using magnetic bead-based electrochemiluminescence *Sensors Actuators B: Chem.* **149** 221-5
[25] Ohno Y, Maehashi K and Matsumoto K 2010 Label-Free Biosensors Based on Aptamer-Modified Graphene Field-Effect Transistors *J. Am. Chem. Soc.* **132** 18012-3
[26] Heller I, Chatoor S, Männik J, Zevenbergen M A G, Dekker C and Lemay S G 2010 Influence of Electrolyte Composition on Liquid-Gated Carbon Nanotube and Graphene Transistors *J. Am. Chem. Soc.* **132** 17149-56

[27] Kim B, Lee J, Namgung S, Kim J, Park J Y, Lee M-S and Hong S 2012 DNA sensors based on CNT-FET with floating electrodes *Sensors Actuators B: Chem.* **169** 182-7

[28] Kim E, Oh J-S, Ahn I-S, Park K I and Jang J-H 2011 Magnetically enhanced adeno-associated viral vector delivery for human neural stem cell infection *Biomaterials* **32** 8654-62

[29] Homola J 2003 Present and future of surface plasmon resonance biosensors *Anal. Bioanal. Chem.* **377** 528-39

[30] Junttila I S, Mizukami K, Dickensheets H, Meier-Schellersheim M, Yamane H, Donnelly R P and Paul W E 2008 Tuning sensitivity to IL-4 and IL-13: differential expression of IL-4Rα, IL-13Rα1, and γc regulates relative cytokine sensitivity *J. Exp. Med.* **205** 2595-608

Chapter 4. Reusable Surface Plasmon Resonance Biosensor Chip

4.1. Introduction

Surface plasmon resonance (SPR) biosensors can detect biochemical materials on the surface of sensor through measuring the changes of refractive index.[1-6] Since SPR biosensors can sensitively measure the kinetics and affinity of bimolecular bindings in real-time and without labelling, SPR biosensors can be used for the evaluation of protein-ligand, protein-protein, protein-carbohydrate, or nucleotide hybridization event. Furthermore, SPR structure based SPR imaging (SPRI) sensor could detect the refractive index change of local area, enabling the monitoring of localized substances such as individual cells.[5-7] Using these characteristics, SPR biosensors have been utilized for many research areas such as immune recognition, drug screening, blood analysis, toxic gases monitoring, and disease diagnosis.[8-10]

However, a SPR sensor has a disadvantage for its practical applications. In conventional SPR sensor chip, receptors were immobilized to sensor surface by chemical reaction such as covalent bonding, and immobilized receptors cannot be removed after sensing, which means that a sensor chip can be used only once. So far, there have been various attempts to reuse SPR sensors. First, there has been research to produce an SPR sensor which can be reused by forming and removing the self-assembled monolayer (SAM) on the chip surface.[6] In the method, a SAM consist of 11-mercaptoundecanoic acid (11-MUA) was formed on a sensor chip surface to

immobilize receptors, and the SAM with receptors was chemically removed by ammonia-hydrogen peroxide mixture after sensing. However, the removal of a SAM by a chemical treatment can damage on a sensor surface, which results in signal degradations. Also, reusable SPR sensors based on plasmonic polymers or magnetic particles were reported.[11, 12] Plastic polymer based reusable SPR biosensor has plasmonic polymer patterns on the surface of the sensor, and they can immobilize receptors and can be removed by chemical treatments. In magnetic particle based SPR biosensor, receptors functionalized magnetic particles were trapped on the surface of sensor by magnetic fields and released by the removal of magnetic field after sensing. However, the polymer based SPR sensor required a dedicated system and lithography processes, and the magnetic particle based SPR sensor required a device generating magnetic fields, which made they difficult to apply these sensors to commercial SPR sensor systems.Herein, we developed a method for building a reusable and multi-target detectable SPR sensor chip. A reusable SPR biosensor chip is a structure that is a ferromagnetic nickel patterned Au/glass substrate holding receptor functionalized superparamagnetic particles. Through the control of external magnetic field, magnetic particles can be trapped and fixed on a nickel patterned Au/glass substrate and can be removed from the substrate after sensing, which enables the reuse of the sensor chip. We verified the basic surface plasmonic properties of nickel patterned Au/glass substrate by a sensing experiment and a UV-VIS spectra measurement. We also showed

the repetitive trap and release of magnetic particles on an Au/glass substrate. Using a reusable SPR biosensor chip, we repeated the detection of H1N1 nucleoprotein (NP) from 3e-7 g/ml to 1e-5g/ml seven times. Despite repeated measurements, the magnitude of detection signals maintained. Moreover, it was demonstrated that our single sensor chip can be used for multi target detection. By changing the types of receptor, we could detect NP antigen and IL-13 antigen with high selectivity. Our method to build reusable SPR biosensors is very simple but powerful since our reusable SPR sensor chip is compatible with conventional SPR system, and it just need a nickel pattern fabrication on conventional SPR sensor chip structure and a magnetic particle control using magnetic field. Thus, our method could be a breakthrough which can bring rather expensive SPR sensor chips to practical applications.

4.2. Experimental Methods

4.2.1 Materials

Superparamagnetic nanoparticle (nano-screenMAG-CMX) was purchased from Chemicell GmbH (Germany). The hydrodynamic size of magnetic particle was about 100 nm, and the surface of magnetic particle was covered with carboxymethyl-dextran (CMX) having a carboxyl group. 1-Ethyl-3-(3-dimethylaminopropyl) carbodiimide hydrochloride (EDC), N-Hydroxysuccinimide (NHS), and Ethanolamine hydrochloride-NaOH was purchased from GE Healthcare (Sweden). The EDC-NHS was used for the

functionalization of magnetic particle by antibody. SIA KIT Au containing a SPR support, double sided adhesive tape, and a protective sheath was also purchased from GE Healthcare. Monoclonal Influenza type A H1N1 Nucleoprotein (NP) antibody and its corresponding antigen were provided from H-Guard Research Center.

4.2.2 Fabrication of nickel patterned reusable SPR sensor chip.

4 inch glass wafers were purchased from Namkang Hi-Tech co.,ltd (Korea). First, the Cr/Au film of 5 nm/45 nm thickness was fabricated on a glass wafer by a thermal evaporation. On this substrate, Ni/Au patterns (5×10 um) of 50 nm/10 nm thickness was fabricated by the photolithography and thermal evaporation. First, a negative photoresist DNR-L300-30 (Dongjin Semichem Co., Ltd., Korea) was coated to an Au deposited glass substrate by a spin coater. The substrate was baked at 110 ℃ for 100 secs. After that, UV light exposed the substrate through photomask in a mask aligner. After exposure, the substrate was baked again at 110 ℃ for 100 secs and dipped in a developer solution. Afterwards, a Ni/Au film was deposited by a thermal evaporator, and lift off process was conducted in acetone. Finally, the substrate was diced by dicing saw.

4.2.3 Repetitive sensing process using nickel patterned reusable SPR sensor chip.

First, a nickel patterned SPR sensor chip was attached to a SPR chip

support by double sided adhesive tape. A 100 μl solution of 0.25 mg/ml magnetic particle was introduced on the nickel patterned SPR sensor chip. Here, an external magnetic field of 150 mT was applied by a neodymium magnet for 1 min. After that, the sensor chip was slightly washed with PBS, and remained solution was removed by a tissue. Then, the sensor chip was installed to a protective sheath and inserted to a SPR detection system (Biacore T100, GE Healthcare). Inside the SPR detection system the sensor chip connected to the microfluidics, and buffer solution (PBS) was flowed to stabilize the sensor chip for 5 min. After stabilization, a 0.1 M EDC and 0.4 M NHS mixed solution was introduced to the sensor chip to activate the carboxyl group of magnetic particle. Later, an antibody solution of 50 μl /ml was introduced and immobilized on the magnetic particle. 1 M ethanolamine solution was injected to block the remaining activated carboxyl group of the magnetic particle. For the detection of target molecule, target molecules were introduced for 300 secs, and buffer solution was introduced for 200 secs to remove non-specifically bound target molecule. Then, we calculated the target signal as difference between before injection and after remove. The detection process was continuously performed from low concentration to high concentration target molecules. After sensing, we took out the sensor chip from the SPR system applied magnetic field of 35 mT opposite direction to the previous applied magnetic field. Here, the sensor chip was washed with DI water for 1 min and dried. In order to detect again, the process described above was repeated.

4.3. Reuse Process of Nickel Patterned Reusable Biosensors

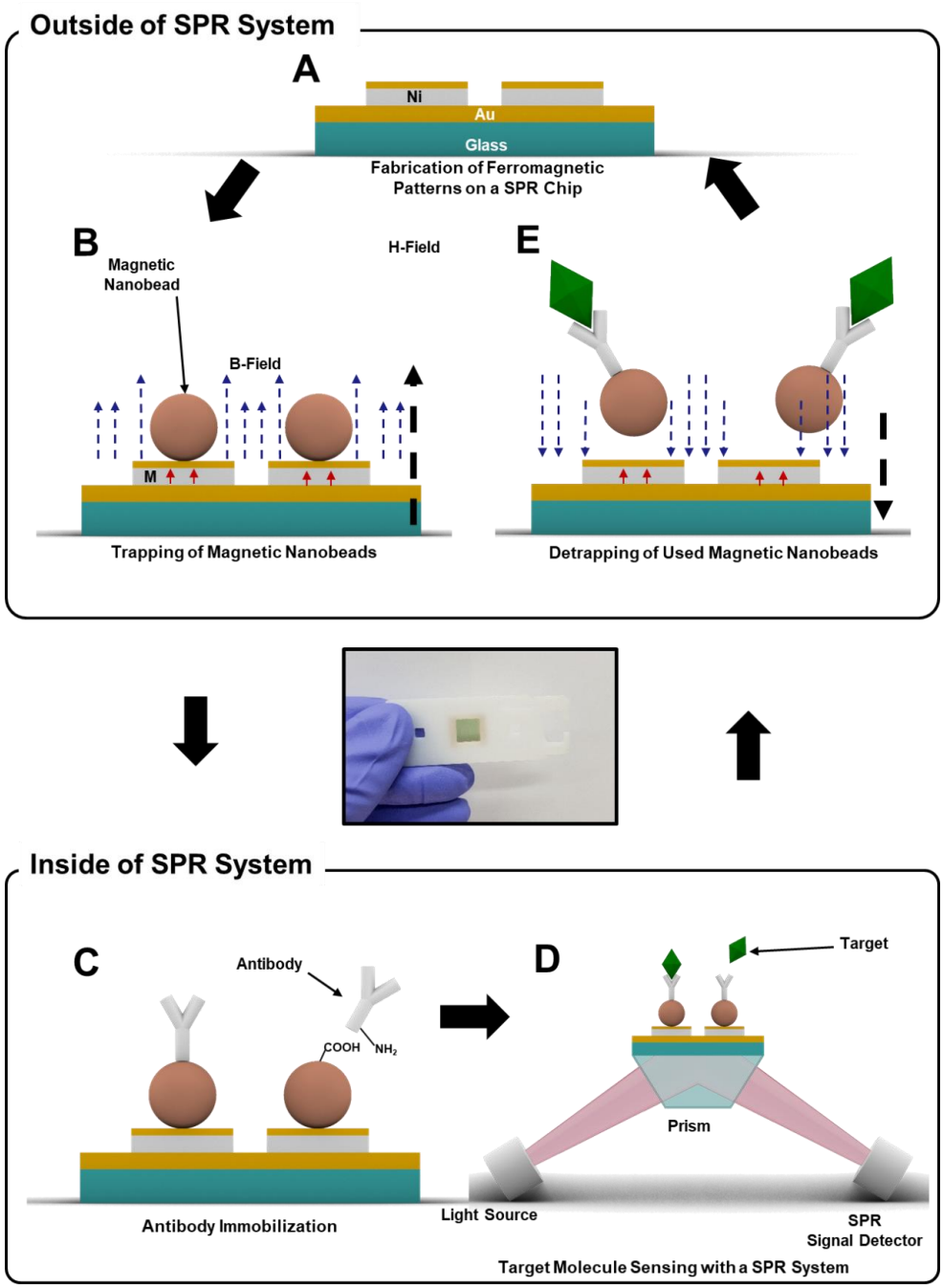

Figure 4-1. Schematic diagram depicting the cyclic process of reusable SPR bio sensor chip using ferromagnetic patterns. (A) Fabrication of ferromagnetic nickel patterns on a conventional SPR chip. (B)Trapping of

magnetic nanobeads on the nickel patterned SPR chip through an external magnetic field. (C) Immobilization of antibodies on magnetic nanobeads using EDC-NHS coupling in SPR system. (D) Detection of target molecules. (E) Removal of magnetic beads using an external magnetic field.

Figure 4-1 shows a schematic diagram depicting repetitive sensing processes of a nickel patterned reusable SPR biosensor chip. First, a Cr/Au film of 5 nm/45 nm thickness was deposited on a glass substrate by a thermal evaporation. The Cr/Au-coated substrate is identical to a conventional SPR sensor chip. A Ni/Au pattern array of 30 nm/10 nm thickness and 10 μm ×5 μm size was fabricated on the substrate by a photo lithography and a thermal evaporation process (Figure 4-1A). An Au layer on the nickel pattern array was used to prevent the oxidation of nickel. The substrate was attached to SPR chip support (Biacore, GE Healthcare) using double sided adhesive tape (center of Figure 4-1). A carboxylic acid functionalized magnetic particle solution was introduced on the chip for a trapping process. Here, an external magnetic field (H-field, 150mT) was applied on the substrate with perpendicular direction to the chip (Figure 4-1B). The external magnetic field magnetized the ferromagnetic nickel pattern (red arrow), which changed magnetic field near the pattern stronger than other region. Thus, the magnetic particles were trapped on the nickel pattern array. After that, the chip was slightly washed with PBS to remove non-trapped particles. In spite of the washing process, the trapped magnetic

particles were remained by a magnetic field from the nickel pattern array. The substrate was installed into a protective sheath, and they were inserted into a SPR system. In the SPR system, a PBS solution flowed through a micro fluidic channel to stabilize a sensor signal. The carboxyl groups of magnetic particles on the nickel pattern were activated by a mixed solution of 0.1 M EDC and 0.4 M NHS. As a result, the carboxyl groups was displaced by succinimide ester groups which could react to the amine groups of antibodies forming covalent bindings with the magnetic particles (Figure 4-1C). After the immobilization, a 1 M ethanolamine solution was introduced to passivate remaining succinimide ester group. After that, a target molecule solution was introduced for a specific sensing (Figure 4-1D). Then, the changes of refractive index near the sensor chip surface were measured in unit called RU (resonance unit). After the sensing, the sensor chip was ejected from the SPR system. For the removal of used magnetic particles, an external magnetic field was applied to the sensor chip with an opposite direction to the magnetization of a nickel pattern (Figure 4-1E). The magnitude of external magnetic field was not strong enough to change the direction of magnetization of nickel pattern. Thus, total magnetic field above the nickel pattern became weaker than those of other region. Due to the magnetic field gradient, the magnetic particles were washed out from the sensor chip. Then, the sensor chip was washed with DI water. As a result, the sensor chip returned to its initial condition without magnetic particles and could be used for the next sensing of target molecule. Based on above

method, we performed such cyclic processes repeatedly for the demonstration of our reusable sensor chip.

4.4. Sensor Structure and Response of a Nickel Patterned SPR Biosensor Chip

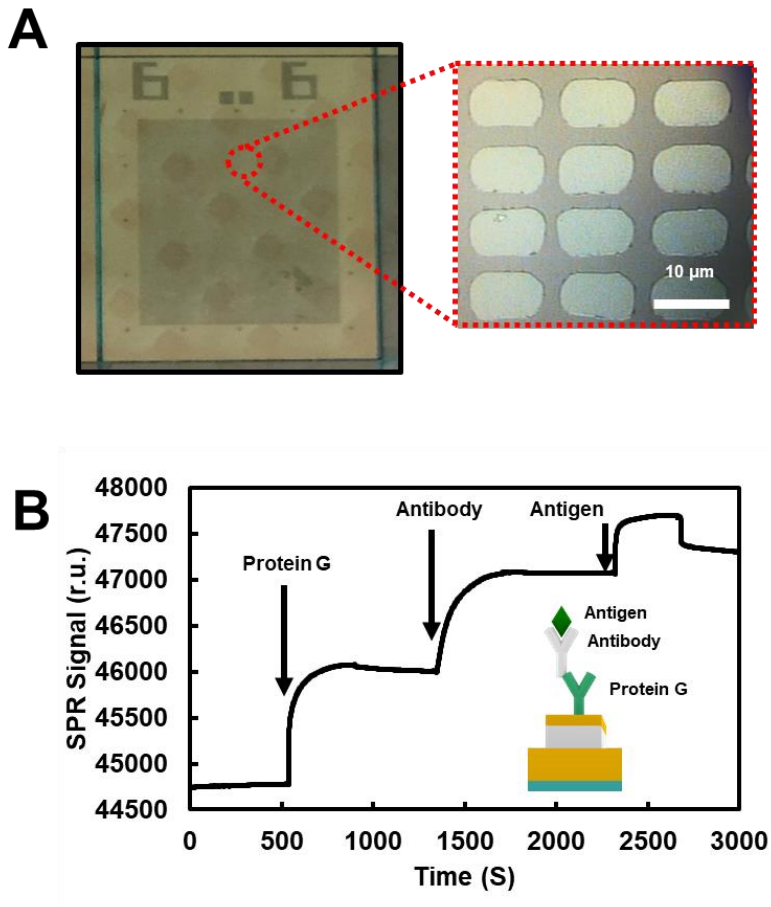

Figure 4-2. Nickel patterns on an Au film on glass substrate and its characteristics. (A) Optical image of a nickel patterned array. Darker colored region means the pattern array. Right red square shows the magnified pattern image from left image. (B) Real-time sensing of CRP antigen using nickel patterned structure.

Figure 4-2 (A) shows the image of nickel patterned SPR sensor chip and its magnified image (red dotted square). Darker square region means a ferromagnetic nickel pattern array. When the sensor chip was attached to a chip support, only the patterned region was exposed, and a microfluidics channel passed through the region. Red dotted circle is magnified and displayed on the right red square. White square shows each nickel pattern whose size is about 10×5 μm. These patterns were used for the tapping of magnetic particles.

Figure 4-2 (B) shows a sensor response when a sensing process of a conventional SPR sensor was conducted using a nickel patterned sensor chip. The experimental procedure is as follows. First, the protein G solution of 0.1 mg/ml that cysteine attached on the N terminal was flowed for 350 secs. Since the cysteine group forms sulfide or disulfide bonding with a gold surface, the protein G attached to the gold surface of a sensor chip. Afterwards, the buffer solution was flowed to remove the non-specific bound protein G and stabilize a signal. After that, the corresponding C-reactive protein (CRP) antibody solution of 0.1 mg/ml and the buffer was flowed for 350 secs and 500 secs, respectively. After that, a CRP antigen solution of 5 μg/ml was flowed for 350 secs, and the buffer solution was flowed. Then we determined the signal by looking difference between the signal before and after the passage. Each protein G and antibody were attached to about 1000 RU, and antigen was attached to about 230 RU. It

should be hard to obtain the sensing signal because surface plasmon resonance signal between glass and gold surface could be changed by the manufactured structure. However, it can be seen that the structure can detect even if the nickel pattern was fabricated. This result indicates that our nickel patterned structure can be used as an SPR sensor.

4.5. Characteristics of a Nickel Patterned SPR Chips

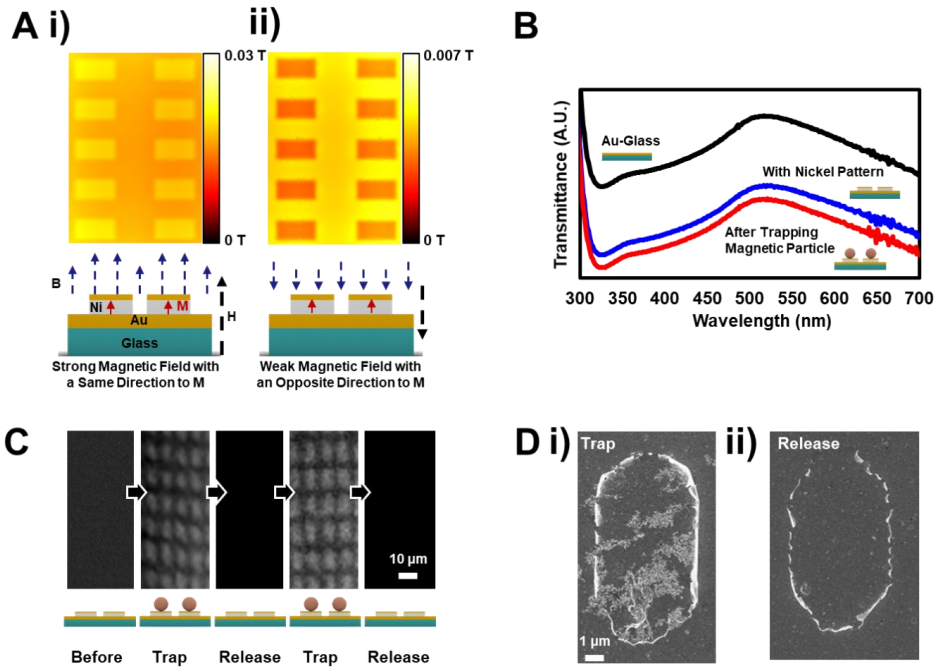

Figure 4-3. Characteristics of a nickel patterned reusable SPR chip. (A)Magnetic field simulation on a nickel patterned structure when the trap (i) and release (ii) of magnetic bead. (B) UV-vis spectra of Au film on glass substrate, Ni patterned Au film on glass substrate, and magnetic beads trapped Ni patterned substrate. (C) Sequential process of trap and release of fluorescence magnetic beads on Ni patterned substrate. (D) SEM image after trapping magnetic beads (i) and releasing (ii) on a nickel pattern.

Figure 4-3 (a) shows the simulation result of magnetic field distributions according to the applied magnetic fields at 1 mm above the

nickel pattern and the schematic diagrams of a simulation situation. The stronger the intensity of a magnetic field, the brighter a color was expressed in the graph. Figure 4-3 (a)-i shows a magnetic field distribution when a strong magnetic field was applied to a ferromagnetic pattern. Since the external magnetic field and magnetic field radiated from the magnetization of nickel pattern were combined, the total magnetic field near the pattern became relatively stronger than those of other regions. This magnetic field gradient generated a magnetic force that attracts paramagnetic materials such as magnetic nanoparticles. [13] On the other hands, figure 4-3 (a)-ii shows a result when the magnetic field in the opposite direction to the magnetization direction is applied. The magnetic field of the region above the ferromagnetic pattern is weaker than that of the surrounding portion. Since ferromagnetic materials have hysteresis characteristics for magnetization, they maintain the magnetization direction in weak magnetic fields. Therefore, the magnetic field near the nickel pattern is canceled and becomes weaker than the surrounding area. This forces the magnetic particles on the nickel pattern to come out of the pattern. This simulation results shows that we can control the trap and release of magnetic particles on ferromagnetic pattern via external magnetic fields.

Figure 4-3 (B) shows UV-VIS transmission spectra of an Au film deposited on glass substrate and nickel patterned Au film on glass substrate before and after magnetic particles trapping. The peak value of the transmission of the Au film deposited on glass substrate is about 520 nm,

which is similar to the results of previous results.[14, 15] Therefore, the gold film appears to be well organized on the glass substrate. Also, it can be seen that the peak value and shape of transmission of the nickel patterned Au film is almost same. Therefore, it seems that the optical properties of Au film were not changed much by nickel patterned structures. Also, the peak value did not change much after the magnetic particles were trapped. The results show that the nickel pattern and the magnetic particles themselves do not significantly change the optical properties.

Figure 4-3 (C) shows repetitive trap and release of magnetic particles over a nickel patterned chip. The experimental procedure is as follows. First a nickel patterned chip was prepared, and its fluorescence image was obtained by a fluorescence microscope (Before). The fluorescence labeled magnetic particle was prepared, then placed on the chip, and the magnetic field of 150 mT was applied for 1 minute. After that, it was washed lightly with PBS solution. After that, an image was obtained by a fluorescence microscopy (Trap). Thereafter, a magnetic field of 35 mT was applied in the opposite direction, and the chip was washed with DI water at the same time. After that, an image was obtained by a fluorescence microscopy (Release). The above trap and release processes were repeated twice. Fluorescence images at the time of trapping show that magnetic particles are gathered in the shape of a nickel pattern. It is also confirmed that there is no magnetic particle at the time of release. The above results show that the magnetic particles can be efficiently trapped and released repeatedly.

Figure 4-3 (D)-i shows SEM images taken after trapping magnetic particles on a ferromagnetic pattern, and releasing them. The experimental method is as follows. We prepared two nickel patterned substrates. Magnetic particle solutions were placed on each substrate. A strong magnetic fields were applied to each substrate to trap the magnetic particles. Thereafter, one substrate was slightly washed by PBS and then a dried (Trap). On the other hands, a rather weak magnetic field with opposite direction to the magnetization direction of the nickel pattern was applied to another substrate, and the substrate was washed with PBS. After that, the substrate was dried (Release). Two samples were observed via SEM. Trap samples show that the magnetic particles are selectively trapped in the ferromagnetic pattern not the other region. In addition, it can be seen that the magnetic particles are somewhat evenly distributed without locating to any edge. This results indicate that the distance between the magnetic particles and Au film is very close without aggregation, which allows that plasmon signal near magnetic particle can be delivered to a Au/glass interface. Additionally, SEM image of release sample shows that the magnetic particles have disappeared clearly. This means that the nickel patterned structure can be reused

4.6. Repeated Sensing Test Using a Single Reusable SPR Sensor Chip.

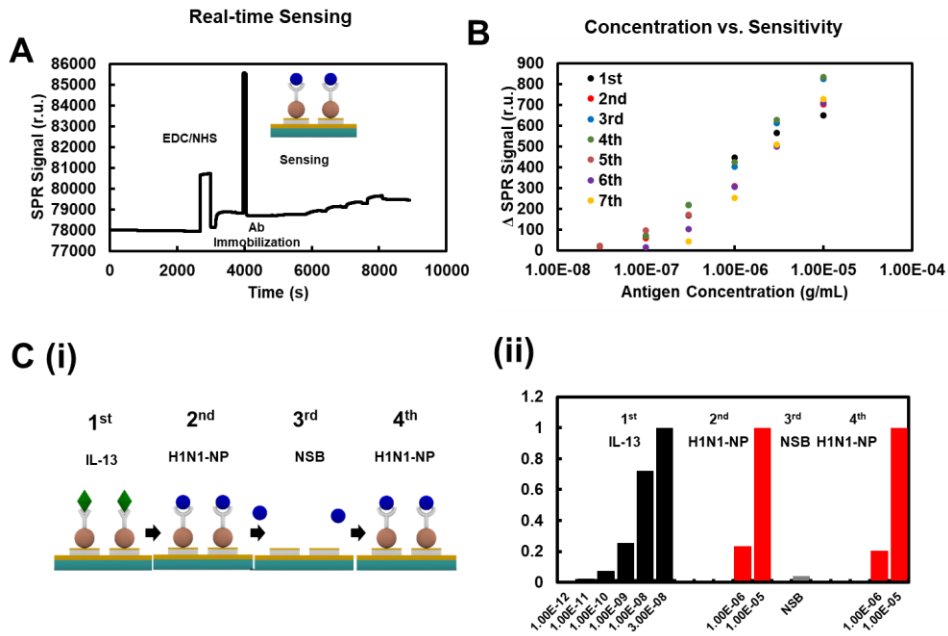

Figure 4-4. Sensing test of reusable SPR biosensor (A) Real time sensing of NP with magnetic beads on Ni patterned reusable SPR chip. (B) Dose dependence comparison of sequential sensing of a reusable SPR chip. (C) Specific detection of two different target molecules. (i) Schematic order of experiment. (ii) Relative dose dependence of IL-13 and H1N1-NP molecule in sequential detection.

Figure 4-4 (A) shows real-time detection graph using a nickel patterned SPR sensor chip. The experimental procedure is as follows. First, a carboxyl group functionalized magnetic particle solution was trapped to the nickel pattern array of a SPR sensor chip by using an external magnetic field. Then, the sensor chip was washed slightly, and remaining water was removed

using a tissue paper. The sensor chip was inserted to a SPR detection system, and a buffer solution was passed through microfluidics channel to stabilize a sensor signal. After few minutes, a mixed solution of 0.1 M EDC and 0.4 M NHS was flowed for about 5 minutes to activate the carboxyl group. Approximately 50 ug/ ml of the H1N1 NP antibody was flowed for 5 min, and antibody and magnetic particles formed covalent bonding. Then, 1 M ethanolamine was flowed for about 1 minute to passivate the remaining NHS group on the magnetic particles. After that, the reaction was examined by flowing the H1N1 NP solution according to the concentration from 3e-7 g/ml to 1e-5g/ml. The results show that the response signal increases as the concentration of NP increases. As a result, the nickel patterned SPR sensor chip could obtain enough detection signals. Thus we applied the sensor chip to the repetitive sensing processes.

Figure 4-4 (B) shows sensor responses according to the concentration of NP in each sensor chip through 7 repeated sensing experiments. We performed sensing experiments with only one sensor chip according to 3e-7 g/ml to 1e-5g/ml of H1N1 NP. After each sensing process, we released the trapped magnetic particles and replaced fresh magnetic particles using external magnetic fields. The graph shows consistent results of 7 repetitive measurements. It can be seen that SPR measurement can be performed many times with one sensor chip.

Figure 4-4 (C) shows the schematic diagram and results of an experiment in which various samples were measured with one nickel

patterned sensor chip. The order of the experiment is as figure 4-4 (C)-i. First, the IL-13 antibody was bound to the magnetic particle on our nickel patterned SPR sensor chip. Afterwards, IL-13 antigen molecule were detected from 1 pg / ml to 30 ng / ml (1^{st} sensing). After sensing and particle washing, an antibody corresponding to H1N1 NP was bound to magnetic particles on the sensor chip, and NP was detected at concentration of 1 ug / ml to 10 ug / ml (2^{nd} sensing). Third, NP protein was detected without adding magnetic particles (3^{rd} sensing). Finally, NP was detected again at concentration of 1 ug / ml to 10 ug / ml (4^{th} sensing). The results were shown as figure 4-4 (C)-ii. First, our sensor chip could detect NP and IL-13 with one sensor chip. A conventional SPR sensor chip usually attaches the receptor in a covalent bonding, which makes it impossible to detect other kinds of target molecules. However, it is possible for our sensor chip to detect various kinds of target materials through replacing magnetic particles. Second, the results of 2^{nd} experiment and 4^{th} experiment show that our sensor chip repeatedly detected NP without degradation of signals by replacing magnetic particles. In addition, the result of the third experiment shows that NP did not absorbed to the nickel patterned SPR chip without magnetic particles, which means that the magnetic particles were clearly removed when release process was conducted.

4.7. Summary

In conclusion, we report a strategy for reusable and multi-detectable

SPR sensor chip by manufacturing a ferromagnetic nickel pattern on a SPR sensor chip. Since ferromagnetic nickel pattern had hysteresis property, we could trap magnetic particles on the nickel pattern and removed the magnetic particles from the nickel pattern using external magnetic field. Through replacing the used magnetic particle to new magnetic particle, our sensor chip could detect another target molecule again. The detection processes were performed for 7 times without degradation of signal in the commercial SPR detection system. Additionally, we could detect two different target molecule only using a single sensor chip through change of receptor molecules on the magnetic particle. We just fabricated a nickel pattern array on a conventional SPR sensor chip structure to reuse the sensor chip. This work provides a simple but quite versatile strategy for building reusable biosensor chips that can be utilized for various practical applications.

4.8. Reference

[1] Morozov V N and Morozova T Y 2006 Active bead-linked immunoassay on protein microarrays *Analytica Chimica Acta* **564** 40-52

[2] Chung J W, Kim S D, Bernhardt R and Pyun J C 2005 Application of SPR biosensor for medical diagnostics of human hepatitis B virus (hHBV) *Sensors and Actuators B: Chemical* **111-112** 416-22

[3] Makaraviciute A, Ramanavicius A and Ramanaviciene A 2015 Development of a reusable protein G based SPR immunosensor for direct human growth hormone detection in real samples *Analytical Methods* **7** 9875-84

[4] Lacy E R 2012 Equilibrium and kinetic analysis of human interleukin-13 and IL-13 receptor alpha-2 complex formation *J Mol Recognit* **25** 184-91

[5] Huygen K, Caboré R N, Maertens K, Van Damme P and Leuridan E 2015 Humoral and cell mediated immune responses to a pertussis containing vaccine in pregnant and nonpregnant women *Vaccine* **33** 4117-23
[6] Hsu H-F, Lin Y-T, Huang Y-T, Lu M-F and Chen C-H 2015 In Situ Regeneration of Si-based ARROW-B Surface Plasmon Resonance Biosensors *Journal of medical and biological engineering* **35** 305-14
[7] El-Kirat-Chatel S, Mil-Homens D, Beaussart A, Fialho A M and Dufrene Y F 2013 Single-molecule atomic force microscopy unravels the binding mechanism of a Burkholderia cenocepacia trimeric autotransporter adhesin *Mol Microbiol* **89** 649-59
[8] Karlsson R, Michaelsson A and Mattsson L 1991 Kinetic analysis of monoclonal antibody-antigen interactions with a new biosensor based analytical system *J Immunol Methods* **145** 229-40
[9] Andrews A L, Holloway J W, Puddicombe S M, Holgate S T and Davies D E 2002 Kinetic analysis of the interleukin-13 receptor complex *J Biol Chem* **277** 46073-8
[10] Karlsson R 1994 Real-time competitive kinetic analysis of interactions between low-molecular-weight ligands in solution and surface-immobilized receptors *Anal Biochem* **221** 142-51
[11] Roche P, Cheung M, Wang S, Banan B, P. Chodavarapu V and Kirk A 2011 *Demonstration of a reusable plasmonic polymer microarray sensing platform* vol 7908
[12] Polyak B, Fishbein I, Chorny M, Alferiev I, Williams D, Yellen B, Friedman G and Levy R J 2008 High field gradient targeting of magnetic nanoparticle-loaded endothelial cells to the surfaces of steel stents *Proc Natl Acad Sci U S A* **105** 698-703
[13] Yoo H, Lee D J, Cho D G, Park J, Nam K W, Cho Y T, Park J Y, Chen X and Hong S 2016 Magnetically-refreshable receptor platform structures for reusable nano-biosensor chips *Nanotechnology* **27** 045502
[14] Siegel J, Lyutakov O, Rybka V, Kolská Z and Švorčík V 2011 Properties of gold nanostructures sputtered on glass *Nanoscale Research Letters* **6** 96
[15] Axelevitch A, Apter B and Golan G 2013 Simulation and expe rimental investigation of optical transparency in gold island fil ms *Opt. Express* **21** 4126-38

Chapter 5. Abstract in Korean

바이오 센서에서의 리셉터는 센서 표면에 화학적으로 고정되어 있고 검지하고자 하는 타겟 물질을 센서 표면에 바인딩 시키는 역할을 수행한다. 이러한 바이오 센서는 근본적인 한계점이 존재하는데 이는 리셉터와 타겟 물질이 반응하는 시간 즉 센서의 반응속도는 타겟물질이 용액상에서 디퓨전 하는 속도에 달려있다는 점이다. 이는 고속의 질병 진단 혹은 하이 쓰루풋과 같은 다량의 검지를 하는 분야에 있어서 제약점이 된다. 또한 한번 검지에 사용된 리셉터는 다시 사용 되기 어려울 뿐만 아니라 화학적으로 센서 표면에 결합되어 있기 때문에 제거가 불가능 하여 센서 칩 전체를 재사용 해야 한다는 어려움이 존재한다. 최근까지 나노 기술을 이용한 바이오 센서들이 개발되고 연구되어 오고 있는데 위에 서술한 단점 때문에 이러한 고성능의 센서들을 상용화 하는 데에 장애물이 되고 있는 실정이다. 본 연구에서는 이러한 현재까지의 바이오 센서의 근본적인 한계들을 극복하는 연구에 대해서 논의하고자 한다.

먼저 자기장 집중형 바이오 칩 구조를 통하여 단층 구조의 자성 나노 입자의 포집과 방출 사이클을 가능하게 하여 검지속도의 향상과 선택성 향상에 대한 논의를 하고자 한다. 선택성이 있는 리셉터가 부착된 자성 입자는 용액상에서 타겟 물질을 고속으로 붙

잡는 역할을 수행하였고 센서 표면으로 포집이 되고 방출이 되었다. 이 때 센서 표면에 있는 또다른 리셉터가 자성 입자가 붙잡은 타겟 물질과 결합하게 된다. 자성 입자가 고속으로 타겟 물질을 붙잡기 때문에 센서의 검지 속도가 향상이 되었고 자기장을 이용한 자성 입자의 방출이 이루어져서 센서의 비선택적 결합을 줄일 수 있었다. 이 방법을 통해 우리는 IL-13 항원의 고속 검지를 수행 하였는데 이는 기존에 소개된 방법의 약 10배 이상의 속도를 보여주고 있다. 게다가 자성 입자의 센서 표면에서의 방출은 비선택적인 흡착을 줄여주는 역할을 하여 선택성과 감도를 높이는 역할을 하였다.

다음으로 자기장을 통한 재사용이 가능한 리셉터 플랫폼 구조에 대해 논의를 하고자 한다. 이 구조는 일반적인 나노바이오 센서 칩을 재사용이 가능하게 만드는 매우 광범위하게 사용될 수 있는 플랫폼이다. 이 구조는 센서를 사용하는 이들에게 쉽게 사용된 리셉터 물질을 제거할 수 있게 해주어서 센서를 재사용할 수 있도록 하는 구조이다. 이 구조를 이용하여 우리는 재사용이 가능한 형광 면역 바이오 센서를 검증하였다. 또한 우리는 우리의 방법이 리셉터를 센서 표면에 매우 가까이 가져갈 수 있다는 점을 보여 주었고 이를 이용하여 센서 표면과 타겟물질간의 거리에 매우 민감한 센서 중의 하나인 카본 나노

튜브 기반의 바이오 센서에 우리의 구조를 적용하였고 이를 검증하였다. 게다가 우리는 또한 하나의 센서에서 우리의 구조를 적용하여 리셉터의 종류를 교체함으로 인해서 여러가지 물질에 대한 검지가 가능하게 됨을 보였다.

마지막으로 기존의 SPR 센서칩 구조에 강자성 니켈 패턴을 제작하여 재사용이 가능하고 여러가지 물질을 검지할수 있는 SPR 센서 칩에 대한 연구에 대해 논의하고자 한다. 자기이력 특성을 가지고 있는 니켈 패턴이 제작된 SPR 센서칩은 자기장을 이용하여 자성 나노 입자를 센서 칩으로 포집을 시킬 수 있고 또한 고정을 시킬 수 있었다. 리셉터는 센서 칩 표면이 아닌 자성 입자에 고정을 시켰기 때문에 자성 입자를 제거하면 리셉터도 같이 제거가 되어서 센서 칩을 재 사용할 수 있었다. 우리는 재사용이 가능한 센서칩을 제작하여 7번의 반복된 검지를 수행할 수 있었고 이 때 센서의 감도는 크게 변하지 않았다. 또한 자성 입자에 부착되는 리셉터의 종류를 변경하는 방식으로 IL-13 항원과 H1N1 바이러스의 핵 단백질을 순차적으로 검지해 낼 수 있었다.

주요어: 자성 나노 입자, 탄소 나노 튜브 전계효과 트랜지스터, SPR 바이오 센서, 강자성, 재사용 센서

학번: 2013-22990